Tectonophysics 762 (2019) 79–96

Contents lists available at ScienceDirect

Tectonophysics

journal homepage: www.elsevier.com/locate/tecto

Impacts of data sampling on the interpretation of normal fault propagation and segment linkage

Tao Ze[a,b,*], Tiago M. Alves[b]

[a] Key Laboratory of Tectonics and Petroleum Resources, Ministry of Education, China University of Geosciences, Wuhan 430074, China
[b] 3D Seismic Lab – School of Earth and Ocean Sciences, Cardiff University, Park Place, Cardiff CF10 3AT, United Kingdom

ARTICLE INFO

Keywords:
Normal faults, fault growth
Data sampling interval
Sampling errors
Fault propagation models

ABSTRACT

Throw-distance (T-D) and throw-depth (T-Z) plots are widely used by researchers and industry to examine the growth of normal faults. This study uses high-quality three-dimensional (3D) seismic and outcrop information to review the effect of data sampling on the interpretation of normal fault growth. The results show that the accuracy of T-D and T-Z data, and of resulting fault slip tendency and leakage factor analyses, are dependent on the sampling strategy followed by interpreters and field geologists, i.e. on a *Sampling Interval/Fault Length Ratio* (δ) for discrete structures. In particular, this work demonstrates that significant geometric changes in T-D plots occur when a *Module Error* (ε_i) for the ratio δ is larger than 6%–9% for faults of all scales and growth histories. This implies that a minimum number of measurements should be gathered on discrete faults to produce accurate T-D and T-Z plots, and that the number of measurements is dependent on fault length. With no prior knowledge of fault segmentation, a δ value of 0.05 should be applied when interpreting faults to fulfil the pre-requisite of a ε_i < 6–9%. In all faults analysed, slip tendency and leakage factors were systematically misrepresented with increasing δ values. To disregard the limits proposed in this work results in: 1) a systematic underrepresentation of the isolated fault growth model, 2) a systematic misrepresentation of fault geometries and related damage zones, 3) the collation of erroneous fault scaling relationships, and 4) ultimately, unreliable interpretations of fault sealing properties. Hence, this work presents a new tool for interpreters and structural geologists to understand the sampling strategies necessary to obtain accurate fault throw and displacement data at different scales of analysis.

1. Introduction

Two end-member models explaining the growth of normal faults are the 'isolated' (Childs et al., 1995; Walsh et al., 2003), and 'constant length' fault models (Cartwright et al., 1995; Cowie and Scholz, 1992; Jackson and Rotevatn, 2013; Morley et al., 1990; Morley, 1999; Rotevatn et al., 2018; Walsh et al., 2002). In the 'isolated' fault model, faults at distinct scales of observation are initially formed by discrete, isolated segments that propagate to link-up laterally with time (Walsh et al., 2003; Ze and Alves, 2016, 2017). In 'constant length' models, faults establish their near-final length at an early stage of their evolution, a phenomenon that is followed by predominant fault propagation in a vertical direction, e.g. dip-linkage reactivation (Cartwright et al., 1995). Complementing the 'isolated' and 'constant length' growth models are faults with relatively large throw-length relationships, i.e. the increasing d_{max}/L ratio of Kim and Sanderson (2005).

The published literature argues that faults formed under the same geological conditions follow either of the end-member fault growth models described above, and that these often occur together in the same region (Fossen and Rotevatn, 2016; Torabi et al., 2019). Importantly, when dealing with fault arrays, geometrical and kinematic coherence can be achieved for distinct fault segments through a combination of growth histories and geometries (Walsh et al., 2003; Mason et al., 2016). This means, in practice, that coherent faults can record discrete segments that grow, at smaller scales, following any of four growth models: 'isolated', 'coherent' through lateral linkage, 'coherent' through dip linkage and 'constant length' models.

A key step in the characterisation of 'isolated' vs. 'constant length' fault growth models is the recognition of fault segmentation (and throw distributions) in 3D via the compilation of systematic throw-distance (T-D) and throw-depth (T-Z) data along the length of resolvable faults (Childs et al., 2003; Baudon and Cartwright, 2008a). The detailed identification of fault segmentation and reactivation has important implications to: 1) the correct understanding of fault propagation

* Corresponding author at: Key Laboratory of Tectonics and Petroleum Resources, Ministry of Education, China University of Geosciences, Wuhan 430074, China.
E-mail address: taoze@cug.edu.cn (Z. Tao).

https://doi.org/10.1016/j.tecto.2019.03.013
Received 9 August 2018; Received in revised form 14 March 2019; Accepted 16 March 2019
Available online 19 March 2019

histories, so that the correct fault growth models are identified (Baudon and Cartwright, 2008a; Giba et al., 2012; Jackson and Rotevatn, 2013), 2) the critical assessment of faults' sealing properties (Lohr et al., 2008; Pei et al., 2015; Seebeck et al., 2014; Worum et al., 2004), 3) the quantification of fault damage zones (Choi et al., 2015; Pei et al., 2015), 4) the assessment of seismic hazards (Pizzi and Galadini, 2009; Turko and Knuepfer, 1991; Zhang et al., 1991), 5) locating ideal CO_2 storage sites (Jung et al., 2014), and 6) the study of sedimentation processes, drainage-systems' evolution and local palaeotopography (Athmer and Luthi, 2011; Booth-Rea et al., 2004; Hemelsdaël and Ford, 2016; Long et al., 2018; Schlische and Withjack, 2009). The sampling strategies adopted by researchers and industry when compiling T-D and T-Z plots can therefore influence the identification of fault segmentation and reactivation, leading to an inappropriate analysis of the six aspects considered above. Incorrect sampling strategies can also lead to gaps in information when analysing the scale relationships of faults at different scales of observation, as shown in Kim and Sanderson (2005) and Torabi and Berg (2011). The adoption of correct sampling strategies has particular importance to the interpretation of faults in seismic data, as seismic resolution (horizontal and vertical) controls how accurately fault geometries are resolved (Manzocchi et al., 2010).

Important methods to identify fault segmentation and reactivation include, but are not limited to: a) the use of structural maps and seismic attributes of key intervals, e.g. RMS amplitude, seismic variance and coherence, so that faults resolved in map view are analysed independently (Alves, 2012; Bahorich and Farmer, 1995; Mattos et al., 2016; Ward et al., 2016; Ze and Alves, 2016), b) displacement analyses that include Throw-Distance (T-D) and Throw-Depth (T-Z) plots (Barnett et al., 1987; Baudon and Cartwright, 2008a; Baudon and Cartwright, 2008b, 2008c; Jackson et al., 2017; Jackson and Rotevatn, 2013; Mattos et al., 2016; Muraoka and Kamata, 1983; Peacock and Sanderson, 1991; Wilson et al., 2013), c) the use of Expansion Indexes in fault analyses (Mohammedyasin et al., 2016; Ze and Alves, 2016), d) studies of fault growth using isochron maps. Geomorphological analyses of knickpoints in rivers crossing active rift basins can also provide constraints on the growth and linkage of fault systems (Whittaker and Walker, 2015). Among these techniques, T-D and T-Z plots are widely used in the identification of fault segmentation and reactivation using 3D seismic data, showing minimal effects of phenomena such as compaction (Taylor et al., 2008), variable sedimentation rates between hanging-wall and footwall strata (Imber et al., 2002), and fault scarp erosion (Van Gent et al., 2010), caveats that often affect Expansion Index and isochron data.

Despite the universal acknowledgment of the latter interpretation caveats by the scientific community, sampling strategies in published T-D and T-Z plots still vary significantly (Baudon and Cartwright, 2008c; Jackson and Rotevatn, 2013; Ryan et al., 2017; Tvedt et al., 2016; Ze and Alves, 2016). In particular, quantitative methods are still lacking in the literature to critically assess the accuracy of T-D plots and ancillary T-Z data when interpreting faults at different scales. In this paper, the focus is on the importance of measuring fault throw (or displacement) data at defined sampling intervals so that accurate T-D and T-Z plots are compiled. Hence, this paper aims to:

1) Critically assess how distinct sampling strategies used to acquire throw (T-Z) data can influence the accuracy of T-D plots in the three dimensions;
2) Understand the possible consequences of compiling unreliable T-D and T-Z plots;
3) Understand the influence of data sampling intervals on the analysis of fault sealing properties;
4) Propose a new quantitative method that seismic interpreters and structural geologists can use to avoid the collection of inaccurate T-D and T-Z data.

Two new parameters are introduced in this work to address these key research questions at different scales of observation, the *Sampling Interval/Fault length Ratio* (δ) and *Module Error* (ε_i) of faults. To better understand the methods proposed in this work, relevant terminology is introduced as follows:

T-D plots

Throw/Distance (or D_{max}/L) plots comprise systematic measurements of throw along the full length of resolved faults on structural maps, seismic data, or outcrops; the 'trace length in map view' as defined by Kim and Sanderson (2005). Maximum throw is measured along the strikes of normal faults or, preferably, interpreters should collect throw-depth (T-Z) data along the fully resolved length of faults to compile T-D plots (Ze and Alves, 2016).

T-Z plots

Throw-Depth plots comprise systematic measurements of throw along fault dips that are completed across the trace of faults by comparing the relative depth of correlative reflections across these same faults (Baudon and Cartwright, 2008c). They provide a record, at depth, of throw variations across a fault surface, from its upper to lower tips. These values are used to compile T-D (or D_{max}/L) plots (Kim and Sanderson, 2005).

Fault length

For structures resolved on seismic data, fault length refers to the longest horizontal or sub-horizontal dimension along a fault plane (Kim and Sanderson, 2005). For faults that are measured in the field, fault length refers to the longest trace of a fault that is exposed at the surface. As the faults analysed in this work have relatively straight exposed traces at the surface (Bristol Channel and SE Crete), and are also clear in the high-quality seismic data from SE Brazil, this study measures faults lengths between their lateral tips (Figs. 1 to 3). This study recognises that truncation and censoring effects occur when acquiring fault length data (Watterson et al., 1996; Torabi and Berg, 2011). However, these will have a minimum impact on our results as later demonstrated in Section 5.

Fault throw

The throw of faults, as observed on seismic data, is the vertical component of fault displacement between correlative hanging-wall and footwall reflections, and is usually represented in milliseconds two-way time (twt) as most seismic data is processed in the time domain (Fig. 3). For faults measured in the field, and later analysed in this work, fault throw refers to the longest trace of a fault measured from a reference surface, either the top of a stratigraphic bed (Bristol Channel, UK) or, in the case of SE Crete, a Holocene reference surface that is traced on both the hanging-wall and footwall blocks of the Ierapetra Fault Zone, SE Crete (Figs. 4 and 5).

Sampling point

Comprises the exact point, along the 'trace length' of faults, at which the throw values are measured; either at its maximum value, or its relative value across a fault surface, i.e. relative to depth along a fault surface.

Sampling interval

Mathematically, the sampling interval in T-D and T-Z plots is the distance, time or depth, at which distinct throw measurements are acquired and recorded. These measurements are obtained along the 'trace length' of a fault and may record strong aliasing due to limited

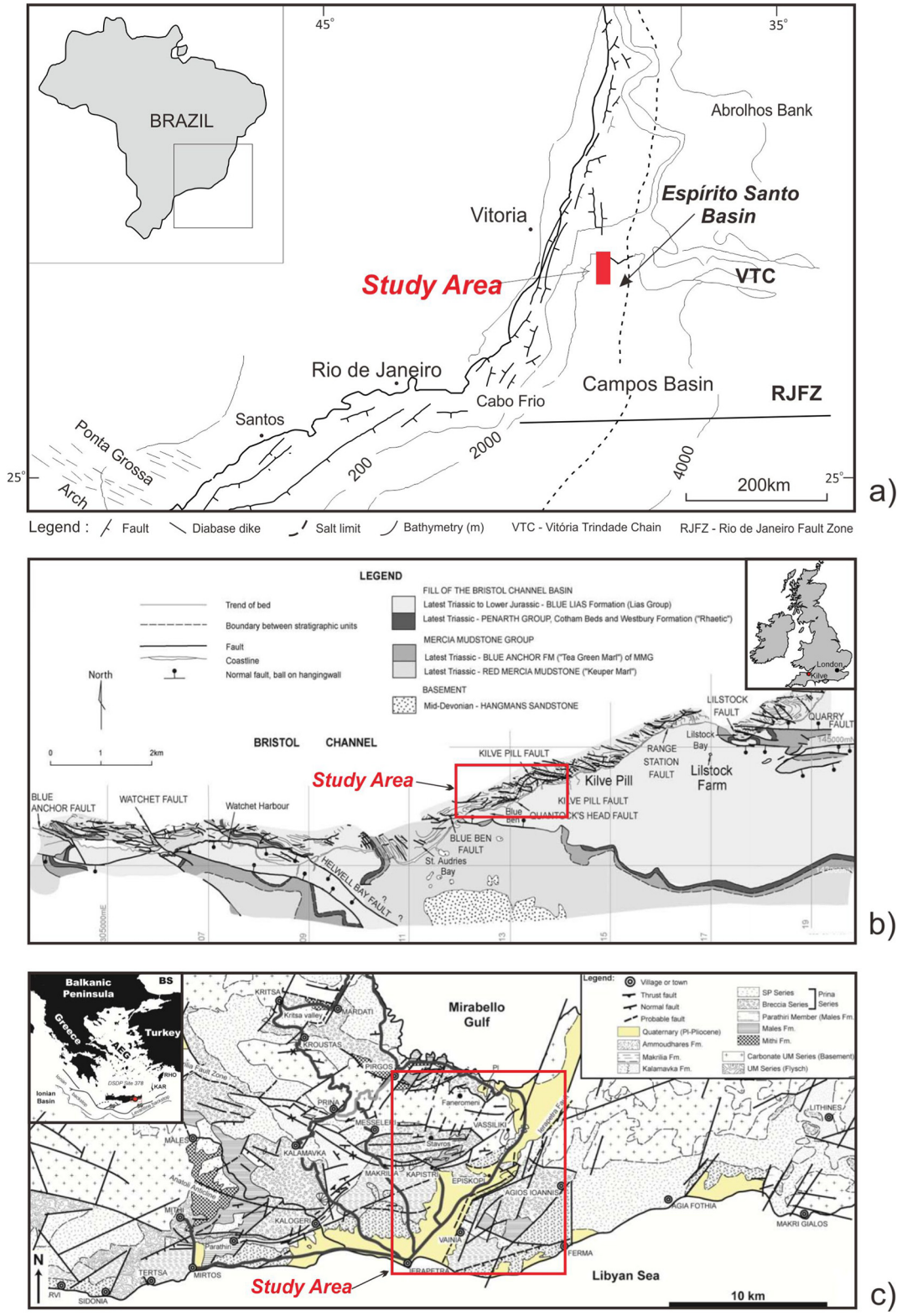

Fig. 1. Location maps of the study areas considered in this work. a) Seismic-scale faults were interpreted in a high-quality 3D seismic volume from the Espírito Santo Basin, SE Brazil. b) Sub-seismic scale faults were analysed on the Somerset coast, Bristol Channel Basin, near the village of Kielve (map modified from Glen et al., 2005). c) Throw data from rift-related faults was acquired from the Ierapetra Fault Zone, SE Crete (map modified from Alves and Cupkovic, 2018).

horizontal resolution in seismic data, data decimation (shot-point spacing), or poor-quality imaging. The sampling interval can also be an important source of inaccuracy in field data if fault throws are sampled at too coarse an interval.

Accuracy

Relates in this work to T-D profiles compiled for a group of faults, using a pre-defined sampling interval, that are compared to accurateT-D profiles measured at the maximum horizontal resolution of a specific

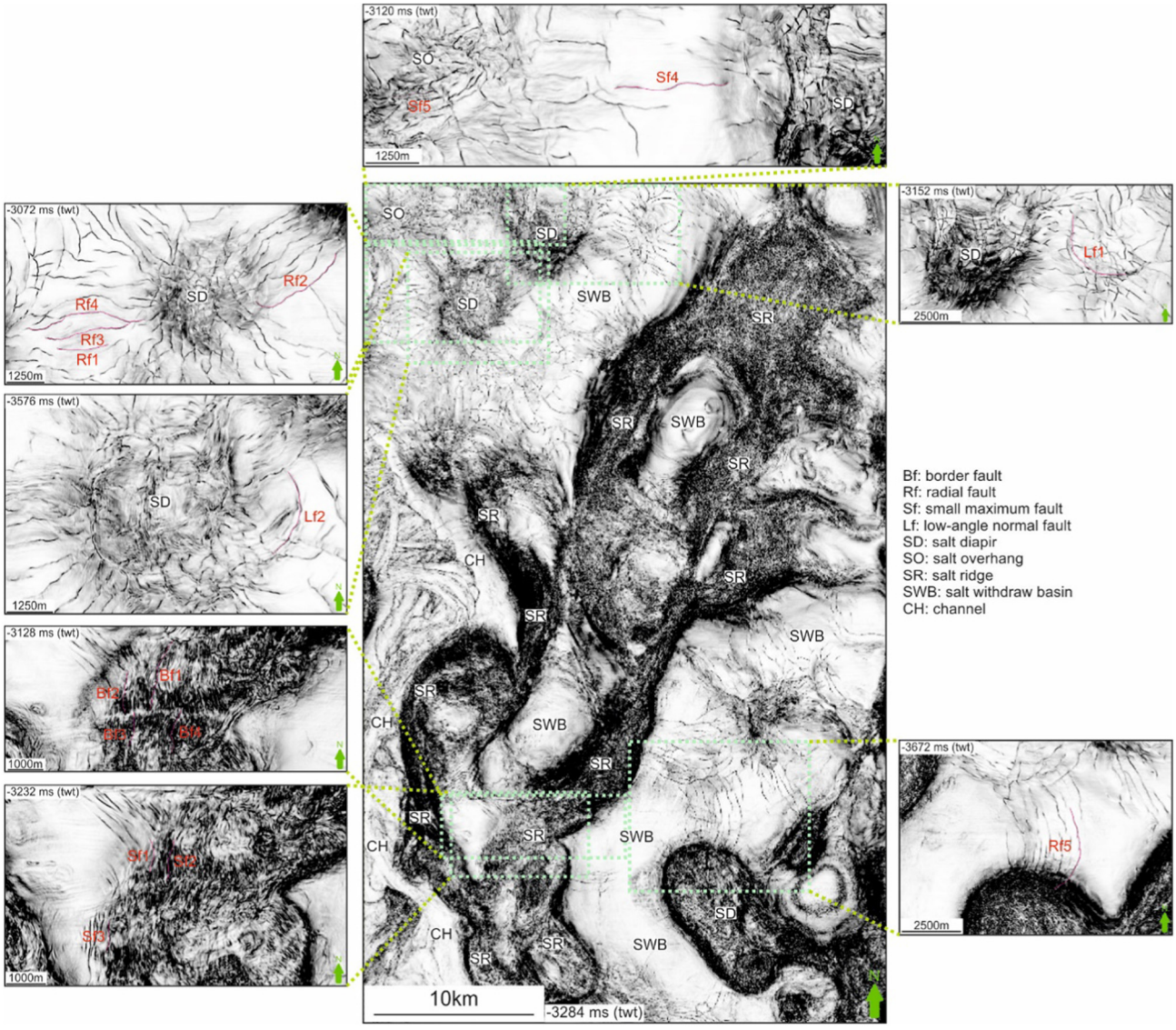

Fig. 2. Variance time slices depicting the faults analysed in this paper. The variance time slices reveal normal faults and diapirs at distinct two-way time (twt) depths. Note the existence of several classes of normal faults associated with halokinesis offshore SE Brazil.

dataset. In practice, accurate T-D (and T-Z) plots are only obtained when minimum differences between the area of a fault segment, and its shape(s), are recorded between these latter plots and those obtained by collecting data at maximum horizontal and vertical resolutions. Small differences in the area of a fault segment, on T-D plots, relate to small *Module Error* (ε_i) values.

Accurate throw-distance profiles

Throw-distance (T-D) plots that are produced reaching maximum data resolution are defined as *accurate* in this work, i.e. T-D plots produced with a sampling interval of 12.5 m for faults interpreted on seismic data. If T-D plots compiled using coarser sampling intervals (lower data resolution) than that representing maximum data resolution have a minimum effect on the identification of fault segmentation, they are also considered as being *accurate*. Otherwise, *inaccurate* T-D plots will be compiled (see Section 3.2).

2. Data sets utilised

2.1. Seismic data

The seismic volume used in this study covers an area of ~1890 km^2 of the Espírito Santo Basin, SE Brazil, and was stacked following a bin (or trace) spacing of 12.5 m (Fig. 1a). Processed to a vertical sampling rate of 2 ms, the vertical resolution of the investigated seismic data can reach 5–8 m near the sea floor and 20 m at the maximum depth of strata investigated in this work (Figs. 1a, 2 and 3). Fifty-nine (59) faults, including crestal faults, radial faults and low-angle normal faults formed on the flanks of salt diapirs, were interpreted every 1, 3, 5, 10 and 20 inline(s)/crossline(s) throughout the seismic volume from SE Brazil (Fig. 2). When needed, composite lines were used to collect throw data perpendicularly to fault-plane dip. The lengths of the interpreted faults range from 225 m to 5000 m, with maximum throw values varying from 6 ms to 73 ms two-way time (twt).

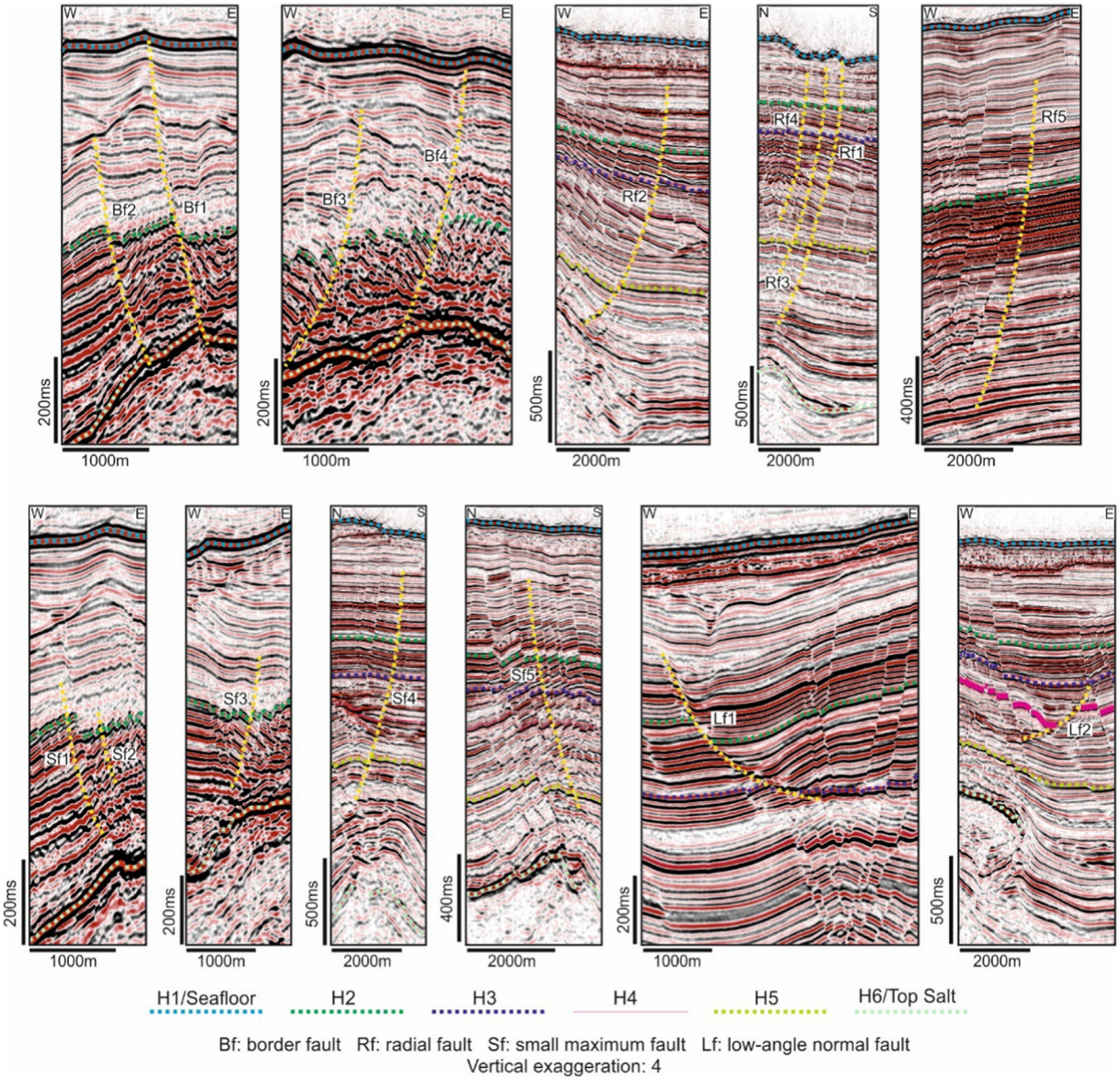

Fig. 3. Seismic profiles showing some of the faults analysed in this paper. The profiles depict the variable geometry of faults in the interpreted seismic volume from SE Brazil, and their relationship with underlying (and flanking) salt structures. Note the vertical propagation of large faults from the top of large salt diapirs in the uppermost seismic profiles.

2.2. Field data

2.2.1. Sub-seismic scale faults from the Somerset Coast (Bristol Channel Basin, United Kingdom)

The tectonic evolution of the Bristol Channel Basin (Fig. 1b) comprises five different stages: 1) N-S extension associated normal faulting and folding during the development of the Bristol Channel in the Mesozoic, 2) reactivation of some of the normal faults formed during stage 1, 3) reverse-reactivation of Mesozoic and older structures in association with the Alpine Orogenic phases (Underhill and Paterson, 1998), 4) reverse-reactivation of normal faults cut by conjugate strike-slip faults (Dart et al., 1995), 5) jointing post-dating the Alpine-related fault reactivation (Rawnsley et al., 1998). Some tectonic reactivation thus occurred in the Bristol Channel Basin during the Cenozoic (Glen et al., 2005), to generate: a) structures formed by N-S contraction that chiefly include reverse reactivated planar normal faults; b) structures formed by east–west contraction; c) intersecting N- to NNW-trending and NE-trending faults. In contrast with the latter strcutures, the faults analysed in the paper were formed by N-S extension, record no apparent tectonic reactivation, and occur in Liassic limestones and shales (see Peacock et al., 2017).

T-D plots for thirteen (13) sub-seismic scale faults - with fault lengths ranging from 1.65 m to 7.55 m and maximum throw values ranging from 3 cm to 29 cm - were measured and interpreted in the field (Figs. 1b, 4a and b). Fault throw measurements in the field depended on how clear they are exposed at the surface. Throw values were measured where the hanging-wall and footwall were exposed on the two sides of the fault trace. The throw-distance measurements were undertaken every 5 cm along the exposed fault trace.

2.2.2. Rift faults from the Ierapetra Fault Zone (SE Crete, Greece)

The Ierapetra Fault Zone is the largest tectonic element in SE Crete, with a length in excess of 25 km, and comprising one of the most active structures on the island (Caputo et al., 2010; Gaki-Papanastassiou et al., 2009) (Figs. 1c and 4c). This fault zone comprises multiple fault segments with a NNE–SSW strike and a dip to the NW, having played a crucial role in the evolution of SE Crete (Gaki-Papanastassiou et al., 2009). The Ierapetra Fault Zone consists of distinct segments with a

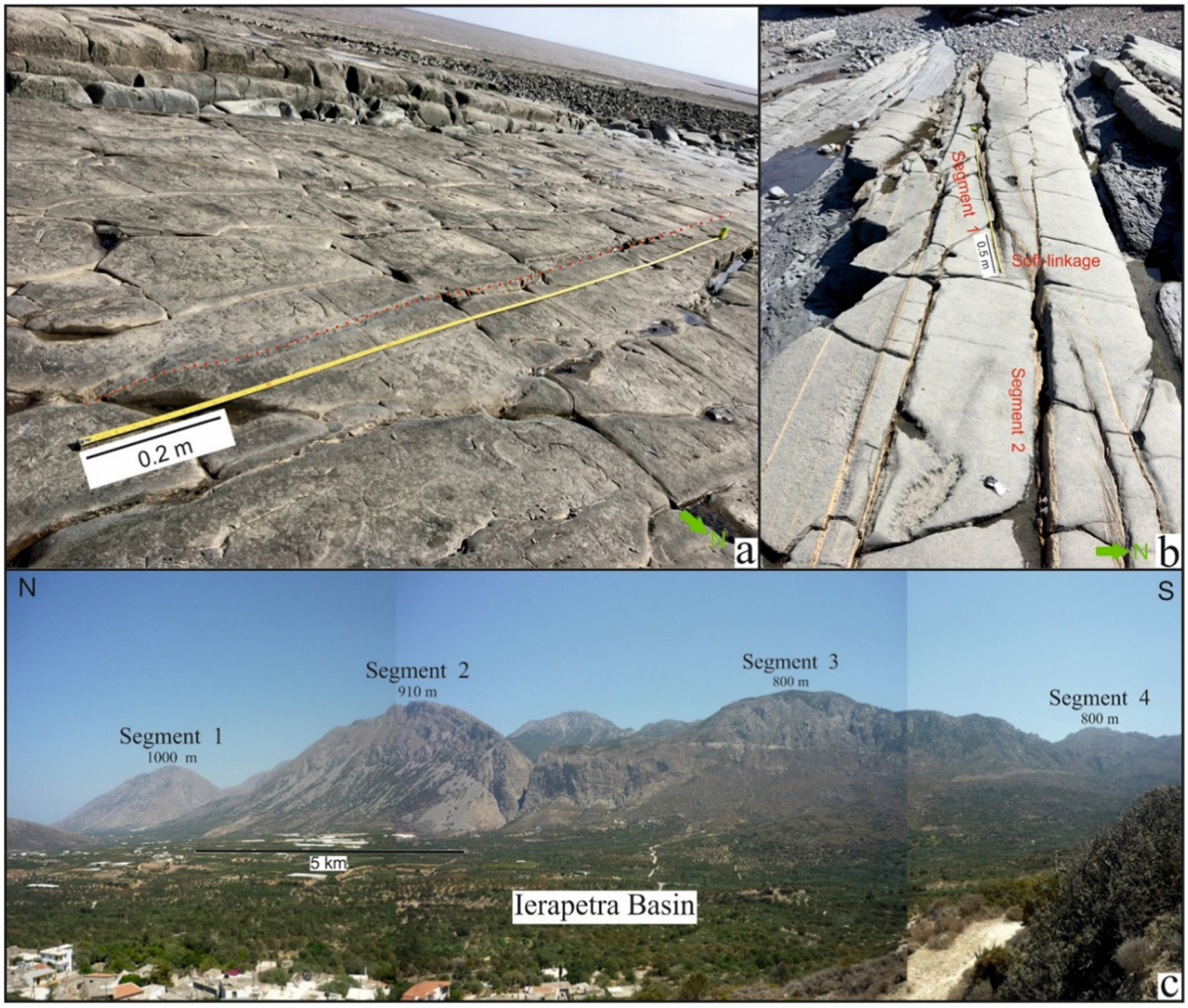

Fig. 4. a) Example of a sub-seismic scale fault comprising a single, isolated fault segment, as analysed in this paper. b) Sub-seismic scale fault comprising two fault segments that are soft-linked, as analysed in this paper. The faults are from the Somerset Coast, Bristol Channel Basin. c) Rift-related fault segments in the Ierapetra Fault Zone, SE Crete.

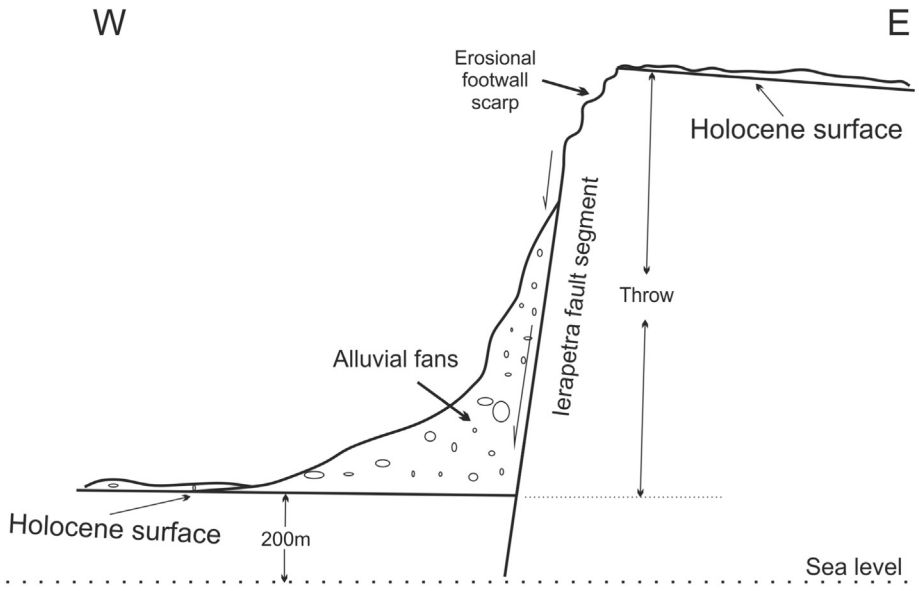

Fig. 5. Schematic representation of how fault throws were systematically measured along the Ierapetra Fault Zone, SE Crete. The throw measurements were taken relative to a correlative Holocene surface that is present on the footwall and hanging-wall blocks of the Ierapetra Fault Zone. The fault scarp of the footwall is partially eroded, and the immediate hanging-wall depocentre to the fault is covered by alluvial deposits. This diagram also recognises the distinct depositional rates that syn-depositional faults record on their hanging-wall and footwall blocks – as well as markedly variable sediment pathways – rendering the use of expansion indexes and layer-by-layer interpretations of throw troublesome on seismic data imaging relatively old, deeply buried rift basins.

step-like arrangement, each one having its own geometry (Gaki-Papanastassiou et al., 2009) (Fig. 1c). Outcropping fault planes are very steep and their lower parts are covered by scree and talus cones (Fig. 4c). Due to its activity, thick sediments cover its hanging-wall, while immediate footwalls are barren of marine sediment and feed adjacent basins at present (Fig. 4c).

Throw-distance (T-D) data for the normal, rift-related fault segments from SE Crete, comprising segment lengths from 7.1 km to 500 m, and maximum throw values between 1000 m and 250 m, are compiled in this work (Figs. 1c and 4c). The total length of the Ierapetra Fault Zone reaches 19.5 km. The approach used in the field was to record the visible throws of exposed fault scarps that have been active since the Late Miocene. Hence, a relatively synchronous Holocene reference horizon was used to compile T-D plots for the outcropping fault segments in the Ierapetra Fault Zone (Fig. 5). During the fault throw mapping we:

(i) Mapped the fault scarps on army maps, namely the present-day height of footwall tips at and any associated erosional and depositional features;
(ii) Collected throw data at a regular interval of 50 m along the fault segments observed in the field.

Throw measurements for rift faults were gathered from 1:50,000 maps from the Hellenic Mapping and Cadastral Organization, on which the geometry of the faults is clear when combined with panoramic photos (Fig. 4c).

3. Methods

3.1. Throw-depth (T-D), slip tendency and leakage factor data

Throw-distance (T-D) profiles are comprehensively used in industry and academia to analyse fault segmentation and document fault propagation histories (Barnett et al., 1987; Baudon and Cartwright, 2008a; Baudon and Cartwright, 2008b, 2008c; Childs et al., 2003; Jackson et al., 2017; Jackson and Rotevatn, 2013; Mattos et al., 2016; Muraoka and Kamata, 1983; Peacock and Sanderson, 1991; Wilson et al., 2013; Cartwright et al., 2000; Ze and Alves, 2016). Faults that comprise one fault segment often present maximum throw values at their centers, diminishing towards their lateral tips (Lohr et al., 2008; Mansfield and Cartwright, 2001; Polit et al., 2009), though some asymmetry in throws can be expected from faults recording oblique slip or some degree of tectonic reactivation (Torabi et al., 2019). Faults that are formed by the lateral linkage of different segments often present several peak values in throw-distance profiles, with lower throw values occurring near the linkage area (Walsh et al., 2003) when these are not fully linked to form a through-going fault zone (Gupta et al., 1998; Finch and Gawthorpe, 2017).

Slip tendency and leakage factors were calculated for all interpreted faults using Midland Valley's 3D Move™. Slip tendency represents the ratio between the shear (τ) and normal (σ_n) stresses acting on a fault (Morris et al., 1996). Leakage Factor comprises a quantitative method to assess the fluid transmissivity of faults, and is calculated as the ratio between the fluid pressure acting on the fault plane and the difference between normal stress and the tensile strength (Valley, 2014). In this work, faults were interpreted on Petrel® and exported to 3D Move™ with fault-stick spacings of 12.5 m, 37.5 m, 62.5 m, 125 m so that we could calculate the slip tendency and leakage factor at different sampling intervals.

3.2. Parameters δ and ε_i to assess the accuracy of T-D plots

This paper introduces two scale-independent parameters for the first time - the *Sampling Interval/Fault length Ratio* (δ) and *Module Error* (ε_i) - to assess the accuracy of T-D plots produced using different sampling intervals. Fig. 6 illustrates the parameters and formulas proposed in this study. Fault length is represented by the parameter n in Fig. 6. The term n represents the sampling interval required to compile T-D plots at maximum data resolution along an horizontal axis. It depends on details such as trace spacing on seismic and the processing parameters of other discrete geophysical data, but it can also be as small as nannometre-size when dealing with microscopic fractures. In non-discrete data (such as outcropping faults), it represents the full length of a fault, from tip to tip (Fig. 6). In turn, the term i represents an arbitrary value for a coarser sampling interval adopted by interpreters when collecting throw data along the full length of a fault, and is usually smaller than n. The smaller the value of i, the closer is the structural interpreter from collecting throw values at maximum data resolution.

A T-D plot sampled at intervals pertaining to maximum data resolution is represented in Fig. 6a. The area bounded by the T-D plot and the horizontal axis is divided into n blocks (n is a positive integer), whose areas are represented by the parameter A_m ($1 \leq m \leq n$, m is an integer) (Fig. 6a).

A T-D plot with a coarser sampling interval of i ($1 < i < n$, i is an integer) is shown in Fig. 6b. The area bounded by this T-D plot, following its horizontal axis, is divided into coarser blocks when compared to Fig. 6a. The area of this T-D plot is represented as A_m' (Fig. 6b).

The difference in area between blocks measured using distinct sampling intervals is represented by the gradient ΔA_m (Fig. 6c), which is calculated as $\Delta A_m = |A_m - A_m'|$. Hence, the *Module Error* (ε_i) represents the ratio between the area of a T-D plot sampled i times (randomly or in a systematic way) below maximum horizontal data resolution, and a T-D plot compiled using sampling intervals that reach maximum horizontal data resolution (Fig. 6c). In these cases, the *Module Error* (ε_i) can be calculated mathematically as:

$$\varepsilon_i = \frac{\sum_1^n |A_m - A_m'|}{\sum_1^n A_m} \quad (1)$$

In Eq. (1), the module $\Delta A_m = |A_m - A_m'|$ represents the absolute error of a measured entity, or value. In such an equation, the *Sampling Interval/Fault length* ratio δ can be calculated as:

$$\delta = i/n \quad (2)$$

An important aspect of our analysis is that T-D plots at maximum data resolution collected data at a spacing of 0.05 km (50 m) for the rift-related faults in SE Crete, 12.5 m for faults imaged on seismic data, and 5 cm for the sub-seismic scale faults in the Bristol Channel. These sampling intervals are represented by the integer 1 in Fig. 5 but can (and should) be naturally changed according to the scale of analysis, e.g. when dealing with smaller shot-point intervals on seismic data or microfractures at the cm or nm scales, for instance.

Apart from measuring fault throw at maximum data resolution, we also aquired throw data every 0.1 km, 0.5 km, 1 km, 1.25 km and 2.5 km for the rift-related faults from SE Crete, every 37.5 m, 62.5 m, 125 m, and 250 m for the seismic-scale faults in SE Brazil, and every 15 cm, 25 cm, 50 cm and 100 cm for sub-seismic scale faults in the Bristol Channel. These throws were used to estimate the threshold *Sampling Interval/Fault Length Ratio* (δ) and *Module Error* (ε_i) values proposed in this work as necessary to compile accurate T-D and T-Z plots (Fig. 6).

4. Effect of sampling intervals on fault analysis

4.1. T-D plots produced at different sampling intervals

This section shows examples of T-D plots produced at different sampling intervals for one discrete fault in SE Crete (Fault A in Fig. 7) and for a fault zone (Ierapetra Fault Zone) composed of five (5) linked fault segments (Fault B in Fig. 7).

For the discrete, isolated Fault A in SE Crete, one fault segment can

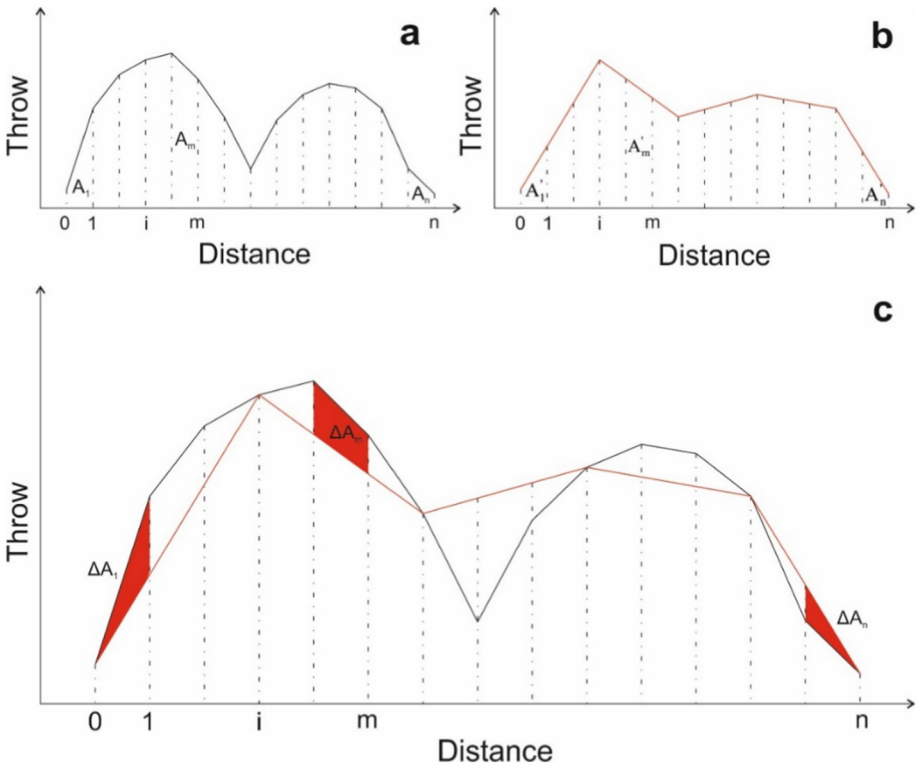

Fig. 6. Schematic map illustrating the parameters defined in Eq. (1), as shown in the text. Fault length is represented by n. a) T-D plot with sampling intervals reaching maximum data resolution, which is represented by the integer 1. The area bounded by the T-D plot and horizontal axis is divided into n blocks (n is a positive integer), represented as A_m ($1 \le m \le n$, m is an integer). 2) T-D plot calculated with a sampling interval of i ($1 < i < n$, i is an integer) that is coarser than maximum data resolution. The area bounded by the T-D plot and horizontal axis is divided into n blocks, represented as A_m'. c) The area difference between blocks with different sampling intervals is represented by ΔA_m, which is calculated as $\Delta A_m = |A_m - A_m'|$. *Module Error* ($\varepsilon_i$), representing the ratio difference between T-D plots with coarser data resolution than that allowed by the data set, and T-D plots compiled with sampling intervals reaching maximum data resolution is calculated as $\varepsilon_i = \frac{\sum_1^n |A_m - A_m'|}{\sum_1^n A_m}$. The *Sampling Interval/Fault Length Ratio* δ is calculated as $\delta = i/n$.

always be identified for all sampling intervals represented in Fig. 7. However, the geometry of Fault A changes significantly when the sampling interval increases to 125 m (Fig. 7-a4). The maximum throw curve (T) shows an arching top with a sampling interval of 12.5 m (Fig. 7-a1). The details shown in Fig. 7-a4 and a5 are quantitatively lost when sampling intervals are significantly larger. The apex of the fault (maximum throw point) also changes (Fig. 7-a4). For Fault A, a maximum sampling interval of 62.5 m is regarded as necessary to obtain accurate T-D plots (Fig. 7-a3), i.e. reflecting accurate fault geometries without losing significant detail.

For Fault B, T-D data gathered at sampling intervals of 50 m identifies five (5) distinct segments with a maximum throw of ~1000 m, as observed in the field (Fig. 7-b1). Important detail is lost in fault segment 1 when the sampling interval increases to 500 m, in effect masking a significant area where fault overlap occurs (Fig. 7-b3). When the sampling interval increases to 1000 m, linkage zones between segments 1 and 2, and segments 2 and 3, are represented by only one minimum throw point. The width and geometry of the fault zone are significantly changed (Fig. 7-b4).

With a sampling interval over 1000 m, maximum throw values are underestimated and fault segment 5 becomes unrecognisable (Fig. 7-b4). When the sampling interval increases to 1250 m, confusion arises between segments 2 and 3, with their linkage zone being represented with one minimum throw in the wrong location (Fig. 7-b5). When the sampling interval increases to 2500 m, only two fault segments can be identified in the entire Ierapetra Fault Zone, while its maximum throw value is underestimated (Fig. 7-b6). A sampling interval of at least 100 m is therefore required to accurately resolve distinct segments this latter fault zone (Fig. 7-b2).

In summary, fault segmentation has a significant effect on the *Module Error* ε_i. Greater *Module Errors* in segmented faults relate to geometric changes in T-D plots in the regions where fault segments are linked (Fig. 7). When increasingly coarse sampling strategies are used to compile T-D plots: 1) fault geometry is significantly changed (Fig. 7-a4, a5, b4, b5 and b6), 2) maximum throws are underestimated (Fig. 7-a5, b4, b5 and b6), 3) fault segmentation is lost on close analysis (Fig. 7-b4, b5 and b6), 4) the geometry of fault linkage points is changed (Fig. 7-b4, b5 and b6), 5) the width of fault linkage zones is underestimated (Fig. 7-b4, b5 and b6), and 6) fault interaction zones (relay ramps, stepovers, hard linkage points) are lost (Fig. 7-b3).

4.2. Relationship between data sampling and accuracy

The accuracy of T-D plots was calculated for 58 faults interpreted on seismic, and 13 sub-seismic scale faults measured in the field (see supplementary data). For the 58 seismic faults analysed, accuracies are 90% (52), 46% (27), 10% (6) and 0% (0) for their respective sampling intervals of 37.5 m, 62.5 m, 125 m and 250 m (Fig. 8a). For the 13 sub-seismic scale faults, accuracies of 100% (13), 38% (5), 7.7% (1), and 0% (0) were calculated for sampling intervals of 15 cm, 25 cm, 50 cm and 100 cm (Fig. 8b).

An important result is that the accuracy of T-D plots for the seismic-scale faults sampled at intervals of 37.5 m (i.e. every 3 shot points) is not 100% (Fig. 8a). In practice, this means that 10% (6) of the faults interpreted in SE Brazil should be measured at sampling intervals of 12.5 m, the maximum horizontal resolution, to be accurately resolved. For the sub-seismic scale faults analysed in the Bristol Channel, measurements undertaken at a spacing smaller than 20 cm are necessary to compile accurate T-D plots (Fig. 8b).

5. Relationships among parameters δ, ε_i and fault geometries

5.1. Relationship between Sampling Interval/Fault Length Ratio (δ) and Module Error (ε_i)

The caveats leading to unreliable T-D plots result in significant errors when estimating fault geometry, i.e. the area of the fault plane delimited by the T-D plots and corresponding horizontal axis (Fig. 6). In order to quantify to what extent natural changes in fault geometry will lead to the compilation of inaccurate T-D plots and, consequently, erroneous fault growth analyses, we calculated the *Module Error* ε_i for all the 73 faults interpreted in this paper following different sampling

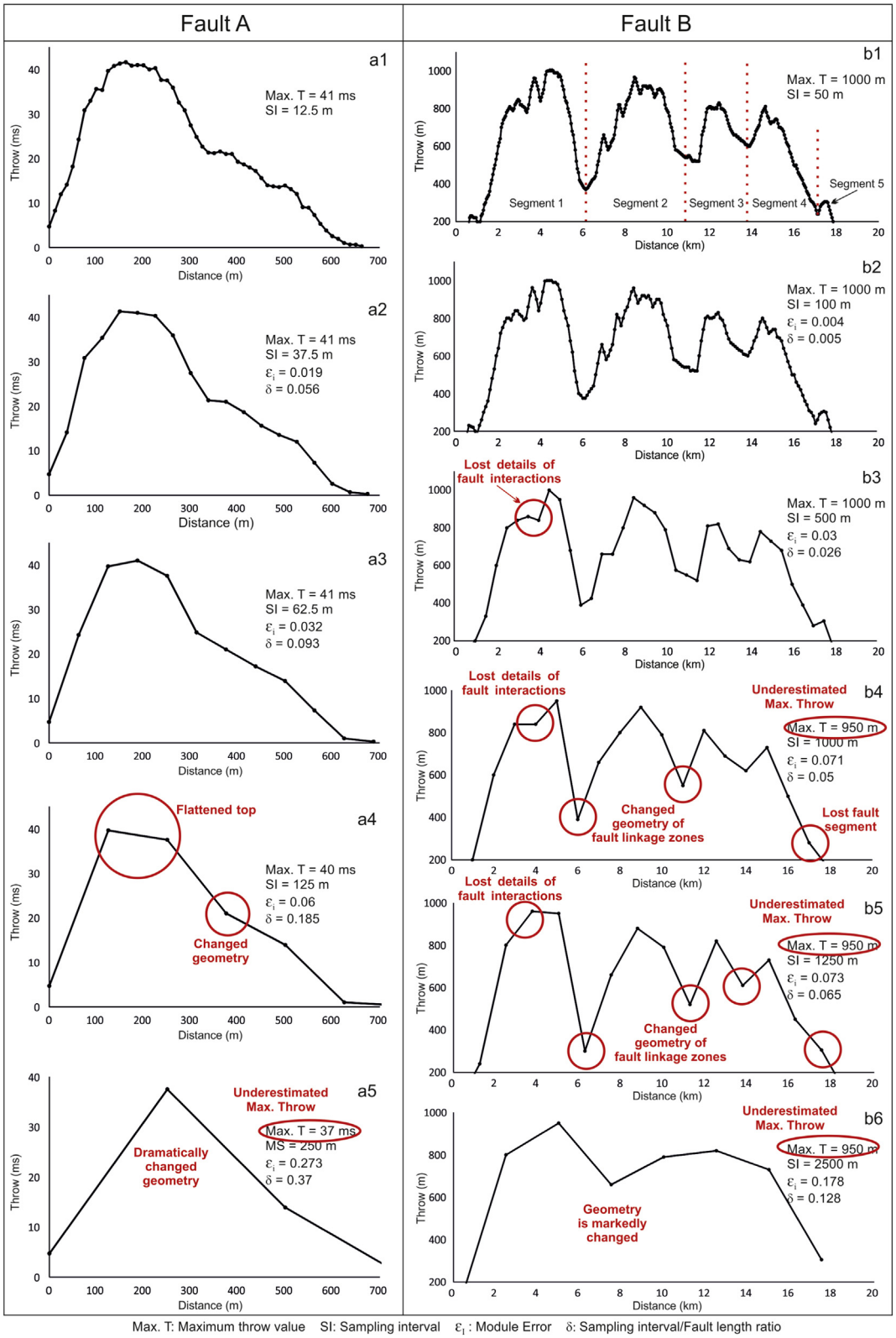

(caption on next page)

intervals (see supplementary data). Due to the fact that fault segment length varies from 1.65 m to 7.2 km for the 73 interpreted faults, the use of a constant sampling interval in structural analyses loses its practical meaning when addressing T-D plot accuracy at distinct scales.

Our results show that the *Module Error* ε_i increases proportionally to the ratio δ (Fig. 9). In order to obtain accurate T-D data from normal faults, ε_i should be < 0.09 (Fig. 9a). Values that are above an ε_i of 0.09 will return inaccurate T-D plots (Fig. 9). The primary value of ε_i for accurate T-D plots varies slightly between seismically resolved faults and the rift-related faults in SE Crete, respectively showing ε_i values of 0.09 and 0.08 (Fig. 9b and c). Though a ε_i value of 0.09 can be suggested as a threshold figure beyond which T-D plots become innacurate,

Fig. 7. T-D plots for faults comprising one fault segment (fault A) and five fault segments (fault B). Both examples are from SE Crete. Fault A has a fault length of 675 m, with a maximum throw value of 41 ms (twt). a1) T-D plot with data acquired every 12.5 m, i.e. the trace spacing of the seismic volume used in this study reveals the most accurate information for fault A. a2) T-D plot for fault A with a sampling interval of 37.5 m, $\varepsilon_i = 0.019$, $\delta = 0.056$. a3) T-D plot for fault A with a sampling interval of 62.5 m, $\varepsilon_i = 0.032$, $\delta = 0.093$. a4) T-D plot for fault A with a sampling interval of 125 m, $\varepsilon_i = 0.06$, $\delta = 0.185$. a5) T-D plot for fault A with a sampling interval of 250 m, $\varepsilon_i = 0.273$, $\delta = 0.37$. b1) T-D plot using data acquired every 50 m for Fault B, revealing the most accurate information. b2) T-D plot for Fault B with a sampling interval of 100 m, $\varepsilon_i = 0.004$, $\delta = 0.005$. b3) T-D plot for Fault B with a sampling interval of 500 m, $\varepsilon_i = 0.03$, $\delta = 0.026$. b4) T-D plot for fault B with a sampling interval of 1000 m, $\varepsilon_i = 0.071$, $\delta = 0.05$. b5) T-D plot for fault B with a sampling interval of 1250 m, $\varepsilon_i = 0.073$, $\delta = 0.065$. b6) T-D plot for fault B with a sampling interval of 2500 m, $\varepsilon_i = 0.178$, $\delta = 0.128$. Note that, for a sampling interval of 125 m in fault A (a4), the maximum throw value is underestimated. The geometry of the fault's maximum throw area and its right-hand side are also significant changed. With a sampling interval of 250 m the calculated T-D plot loses its practical meaning. For Fault B, when sampling interval is 500 m, details of fault segment 1 are lost (red circle in b3) close to a zone of fault interaction. With a sampling interval of 1000 m (b4), the maximum throw value is significantly underestimated, and fault segment 5 is not identified. With a sampling interval over 1250 m (b5 and b6), maximum throw values, fault geometry and fault segmentation are not resolved on the T-D plot. (For interpretation of the references to colour in this figure legend, the reader is referred to the web version of this article.)

92% of the plotted T-D data still show ε_i values below 0.06 in Fig. 9a.

In terms of the *Sampling Interval/Fault Length Ratio* δ, our results show that a threshold value of 0.1 is valid for isolated, discrete faults of all scales, i.e. data sampling should occur at a spacing of < 10% the fault length in order to obtain accurate T-D data for faults composed of only one fault segment (Fig. 9). Yet again, 74% of the analysed faults show δ values that are < 0.06 in Fig. 9a, i.e. sampling should be undertaken at < 6% of the fault length in these isolated, discrete structures, with a percentage of 71% for faults on seismic data requiring $\delta < 0.07$ and 83% of field faults requiring $\delta < 0.06$, respectively, to be accurately discerned on T-D plots (Fig. 9b and c).

In order to postulate a practical threshold δ value to assess the accuracy of structural interpretations, all reliable T-D measurements were selected and differentiated in Fig. 10 according to the first-order fault segments each fault comprises. Our results show a clear difference between isolated and segmented faults when considering the δ values necessary to obtain accurate T-D data (Fig. 10a). A threshold value of $\delta = 0.05$ is shown in Fig. 9 for faults of all scales. This value correlates with threshold values of $\delta = 0.06$ and $\delta = 0.05$ respectively for seismically resolved faults (SE Brazil) and for sub-seismic scale faults (Bristol Channel) (Fig. 10b and c). The $\delta = 0.05$ threshold value suggests that, for faults of any scale, sampling should be undertaken at intervals that are < 5% of the total fault length if they are segmented. Sampling intervals of < 10% of the total fault length are necessary for faults comprising only one fault segment (Fig. 10). However, without previous knowledge of fault segmentation, a δ value of 0.05 is strongly suggested as a minimum, practical threshold value for interpreters and structural geologists when compiling T-D and T-Z data (Fig. 10c).

5.2. Relationship between fault length and the δ ratio

The relationship between fault length and the δ ratio shows a robust power-law relationship; with increasing fault lengths, the threshold value δ necessary to produce reliable T-D plots decreases significantly (Fig. 11). For faults interpreted on seismic, showing a length varying from 275 m to 5000 m, the threshold δ value becomes constant when fault length exceeds 3500 m, and a value of $\delta \sim 0.015$ is indicated in Fig. 11. With longer faults, such as the rift faults in SE Crete, the threshold δ values necessary to obtain accurate T-D data are 0.025 and 0.018 respectively. This proves that, for faults that are longer than 3500 m, a threshold δ value of 0.015 (sampling intervals at < 1.5% of the fault length) provides accurate T-D data (Fig. 11a).

5.3. Relationship between average fault-segment length and Module Error (ε_i)

As indicated in the previous section, in order to obtain reliable T-D plots for rift faults, which have greater fault lengths and average fault-segment lengths, a smaller δ value should be considered by interpreters. Such a result indicates that fault length and average fault segment length influence the final δ values required to produce accurate T-D plots, i.e. too coarse a sampling interval when compiling T-D plots will result in a strong bias towards 'constant length' fault models for large, basin-bounding faults. The relationship between ε_i and average fault segment length shows that, for the interpreted faults on seismic data (SE Brazil), ε_i values decrease relative to longer average fault segment lengths; the *Module Error* ε_i returns values of 1.7%, 2.6%, 4% and 6% respectively for T-D data that are measured every 37.5 m, 62.5 m, 125 m and 250 m (Fig. 12). The *Module Error* (ε_i) for faults below the

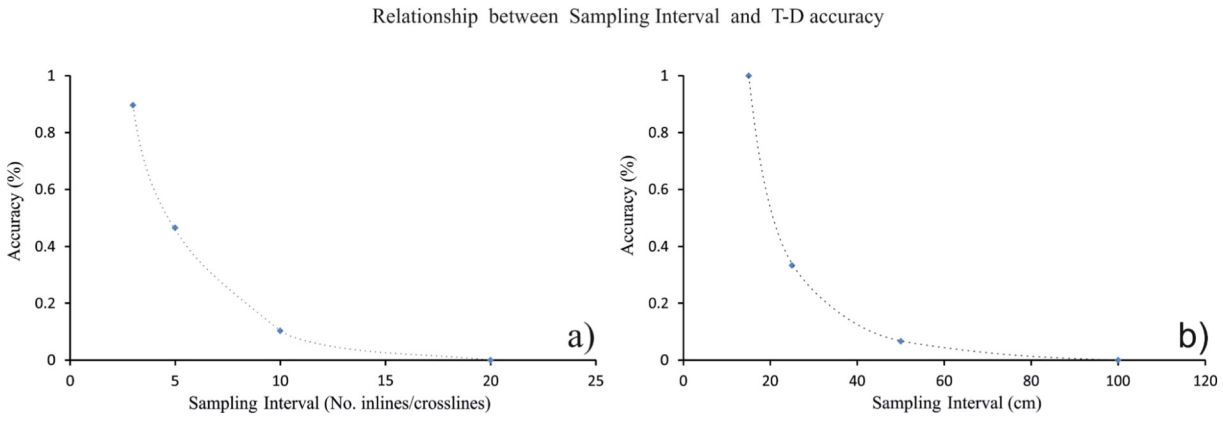

Fig. 8. Relationship between T-D plots' accuracy and sampling interval. For the faults interpreted in the seismic volume from SE Brazil (see graph on the left), with a bin spacing of 12.5 m, T-D plot accuracy decreases dramatically with increasing sampling intervals, showing accuracies of 90%, 46%, 10% and 0%, respectively, for sampling intervals of 37.5 m, 62.5 m, 125 m and 250 m. For sub-seismic scale faults from the Bristol Channel (on the right), accuracy is 100%, 38%, 7.7%, and 0% relative to sampling intervals of 15, 25, 50 and 100 cm. Note that 10% of the T-D plots for faults interpreted on seismic data are inaccurate with a sampling interval of 37.5 m, indicating that some of the faults in SE Brazil have to be measured every 12.5 m – the maximum trace spacing, or bin size - in order to obtain accurate T-D plots.

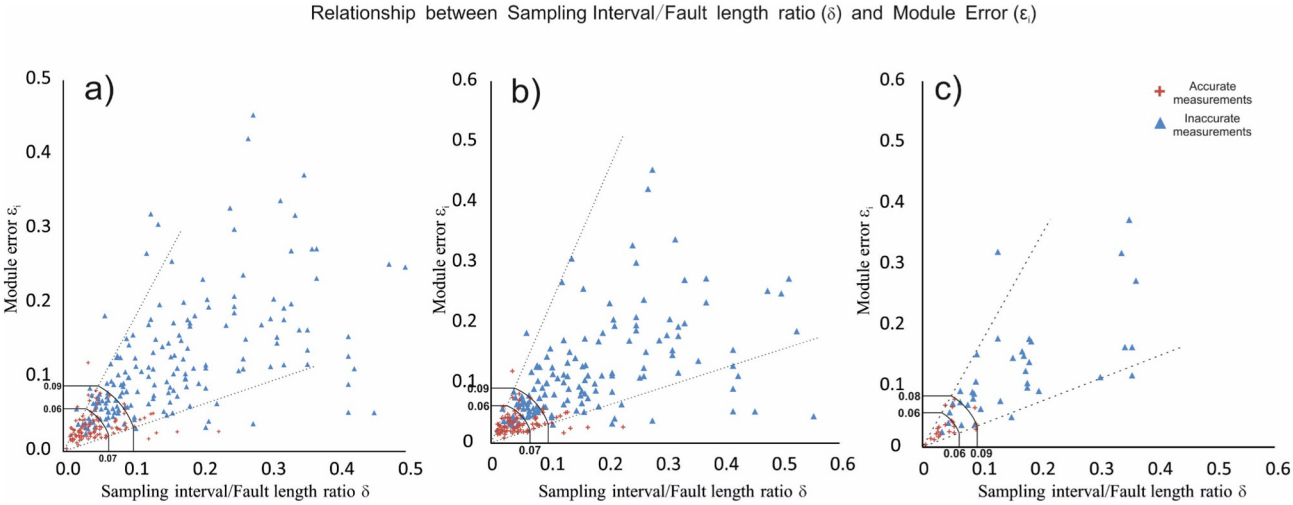

Fig. 9. Relationship between *Sampling Interval/Fault Length Ratio* (δ) and *Module Error* (ε_i). Module error increase rapidly with increasing *Sampling Interval/Fault Length ratios*. a) In order to obtain accurate T-D plots for faults of all scales, the ε_i value should be < 0.09, with a δ value of 0.1. Note that 92% of all accurate measurements are located within a threshold of $\varepsilon_i < 0.06$, $\delta < 0.07$. b) Relationship between δ and ε_i for seismic faults. For accurate T-D plots, $\varepsilon_i < 0.06$ and $\delta < 0.07$ should be applied. c) Relationship between δ and ε_i for sub-seismic scale faults. For accurate T-D plots, $\varepsilon_i < 0.06$ and $\delta < 0.06$ should be applied.

seismic scale also shows a negative correlation with average fault segment lengths (Fig. 12), i.e. *Module Error* decreases with increasing fault segment length.

5.4. Relationship between T-D ratios and δ

In our work, faults composed of discrete fault segments show twice or even three times the length of isolated faults. However, maximum throw values are almost the same, resulting in a smaller T-D ratio. In 'constant length' growth models faults have increasing T-D ratios; fault length reaches its final value very early in the development of a fault, further accumulating vertical fault displacement (i.e. throw) with time. The relationship between the T-D ratio and δ shows that, with a smaller T-D ratio, the values of δ are smaller (Fig. 13). This means that more throw measurements should be undertaken for faults that are composed, at any time in their evolution, of distinct segments; a result consistent with the data described in Section 5.3 (Fig. 10).

6. Effect of data sampling on fault slip tendency and leakage factor analyses

Estimated values of slip tendency and leakage factor under pre-established stress values are dependent on the roughness, geometry and orientation of fault planes relative to the stresses acting on the fault (Lohr et al., 2008). In order to understand the effect of δ on slip tendency and leakage factor analyses, faults from the SE Brazil seismic volume were mapped manually following sampling intervals of 12.5 m, 37.5 m, 62.5 m and 125 m and imported from Petrel® to produce distinct fault models on 3D Move™ (Fig. 14). These fault surfaces were analysed for slip tendency and leakage factor assuming pore pressures of 0 MPa, 5 MPa and 10 MPa (Fig. 14). Our analysis assumes that fault surfaces interpreted every 12.5 m, which is the maximum horizontal resolution of the SE Brazil 3D seismic volume, reveal the most accurate slip tendency and leakage factors. The fault analysed comprises two fault segments (Fig. 14). The two fault segments have similar maximum throw values and lengths (Fig. 14).

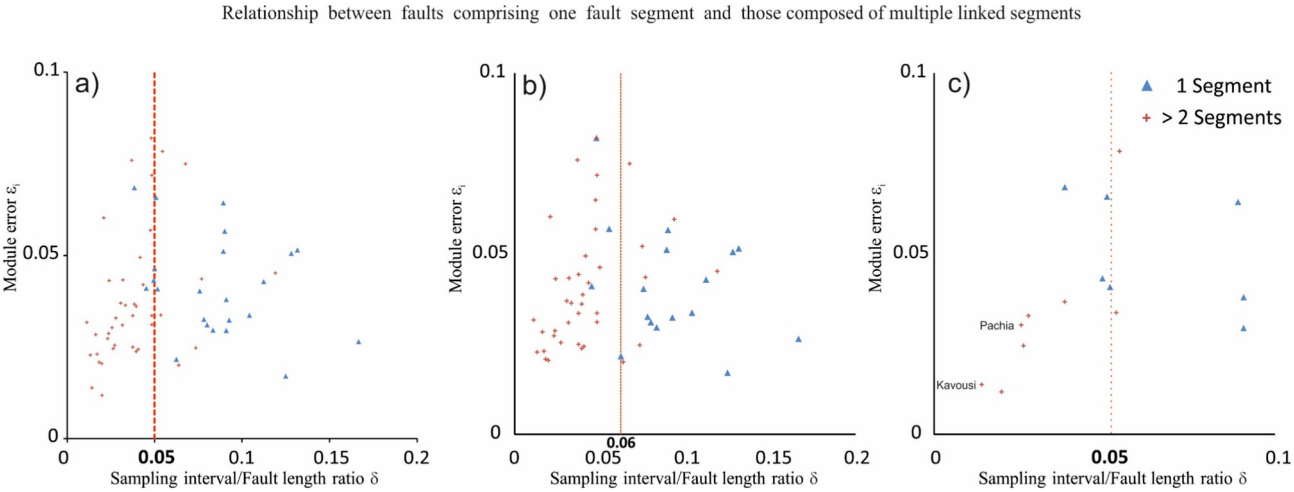

Fig. 10. Accurate *Sampling Interval/Fault Length Ratio* (δ) for faults comprising one fault segment and ≥2 fault segments. a) A boundary of δ = 0.05 is shown for faults of all scales. b) A boundary of δ = 0.06 is shown for the seismic-scale faults in SE Brazil. c) A boundary of δ = 0.05 is shown for faults analysed in the field.

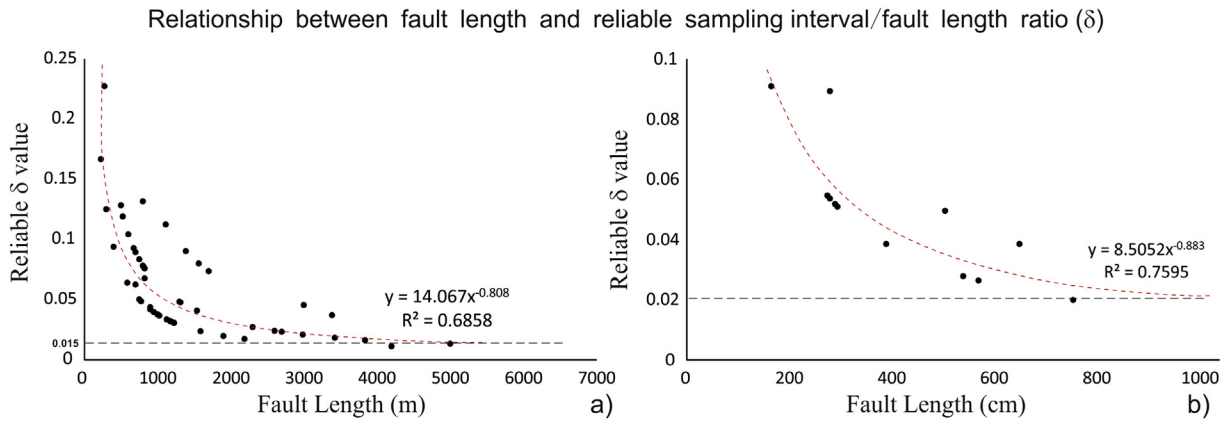

Fig. 11. Relationship between fault length and reliable *Sampling Interval/Fault Length Ratio* (δ). The results indicate a power-law relationship between Fault Length and δ, in which reliable δ values (i.e. returning accurate T-D plots) decrease with longer fault lengths. a) For seismic-scale faults, reliable δ values (δ = 0.015) become constant with fault lengths ≥3500 m. b) For sub-seismic scale faults, reliable values of δ (δ = 0.02) also decrease rapidly with increasing fault lengths.

6.1. Variations in slip tendency for distinct sampling intervals

For a pore pressure value of zero (0) MPa, areas with high slip tendency remain similar on the fault surface interpreted every 37.5 m compared to those of the fault surface interpreted every 12.5 m (Fig. 14-a1 and -a2). However, the magnitude of slip tendency decreases with larger sampling intervals, i.e. with a coarser interpretation (Fig. 14-a2). When the fault was interpreted every 62.5 m, slip tendency in its lower part changed significantly (Fig. 14-a3). When picking faults every 125 m, the fault surface becomes so smooth that slip tendency is markedly underestimated (Fig. 14-a4).

For pore pressure values of 5 MPa and 10 MPa, slip tendency is similar to that calculated assuming pore pressures of zero (0) MPa. With larger sampling intervals: 1) where high slip tendency values occur, they are markedly dispersed (Fig. 14-b2, c2); 2) areas of high slip tendency are lost (Fig. 14-b3, c3); and 3) slip tendency is systematically underestimated (Fig. 14-b4, c4).

6.2. Variations in leakage factors for distinct sampling intervals

For a pore pressure value approaching zero (0) MPa, and when interpreting the fault surface every 12.5 m, leakage factors in its upper part are 0.3–0.4 (Fig. 14-d1). However, these values are reduced to 0.2–0.3 with larger sampling intervals (Fig. 14-d2, d3). In addition, zones of higher leakage factors are narrowed (Fig. 14-d2, d3) and ultimately lost (Fig. 14-d4).

For a pore pressure of 5 MPa, sampling intervals of 62.5 m and 125 m for the fault surface result in systematic underestimations of leakage factors (Fig. 14-e3 and e4). With a sampling interval of 37.5 m, high leakage factors remain similar in distribution, but their magnitude decreases (Fig. 14-e2).

For a pore pressure value of 10 MPa, zones with high leakage factor are the same as with sampling intervals of 12.5 m and 37.5 m. However, leakage factors are relatively lower with a sampling interval of 37.5 m (Fig. 14-f1 and f2). When the sampling interval increases to 62.5 m, there is a systematic overestimation of leakage factors in the lower part of the modelled fault, while the zones with high leakage factor are enlarged (Fig. 14-f3). When the sampling interval increases to 125 m, there are systematic underestimations of both the areas with high leakage factors, and their magnitudes (Fig. 14-f4).

7. Discussion

This paper introduces two new parameters, the *Sampling Interval/Fault Length Ratio* (δ) and *Module Error* (ε_i), as quantitative guidelines for fault analyses. Adopting the threshold values of δ and ε_i suggested in this work will prevent misinterpretations of fault growth histories. The parameter *Module Error* (ε_i) reflects the effect of distinct sampling intervals on the accuracy of fault geometry measured through T-D plots. With *Sampling Interval/Fault Length Ratios* (δ) that do not take into account maximum data resolution, ε_i increases rapidly (Fig. 9). The latter parameter δ is proposed in this paper as key to quality-control the structural analysis of faults at all scales.

7.1. Effects of data sampling on fault growth models

Theoretically, unless throw-distance (T-D) data are obtained using sampling intervals close to maximum data resolution, T-D plots can be significantly distorted (thus reflecting increased ε_i values) in multiple ways (Fig. 15):

1) Fault geometry is significantly changed,
2) Maximum fault throw values are underestimated,
3) Fault segmentation is overlooked,
4) The geometry of fault linkage zone(s) is changed,
5) The width of fault linkage zone is underestimated,
6) Fault interaction zones are lost.

When sampling intervals are coarser, fault throw will likely be misinterpreted where fault segment boundaries occur. In this case, segment linkage will be overlooked and faults wrongly interpreted as representing a 'constant length' fault growth model.

In order to constrain the effect that increasing sampling intervals have on fault geometry, the parameter *Module Error* ε_i is proposed in this work. Our analysis suggests that when ε_i is over 0.09, the geometries of T-D plots are significantly changed, meaning that fault analyses based on these same T-D plots lose their practical meaning. Specifically, ε_i should be well below 0.06, so that 92% of the analysed data are located within this latter threshold value, for distinct fault lengths (Fig. 9).

One of the key factors directly related to fault sealing properties is the roughness of fault planes (Lohr et al., 2008). When modelling slip tendency and leakage factor for faults interpreted on seismic data, geometric details of fault planes rely on both the interpreters' experience when creating fault sticks and corresponding stick sampling interval(s) (Fig. 14). Larger sampling intervals imposing artificial roughness on faults result in erroneous slip tendency and leakage factor analyses (Fig. 14).

Our results show that, under defined pore-pressures, zones of high slip tendency are enlarged when using wider sampling intervals. However, maxima in slip tendency are relatively smaller (Fig. 14). Coarser sampling intervals result in leakage factors being systematically

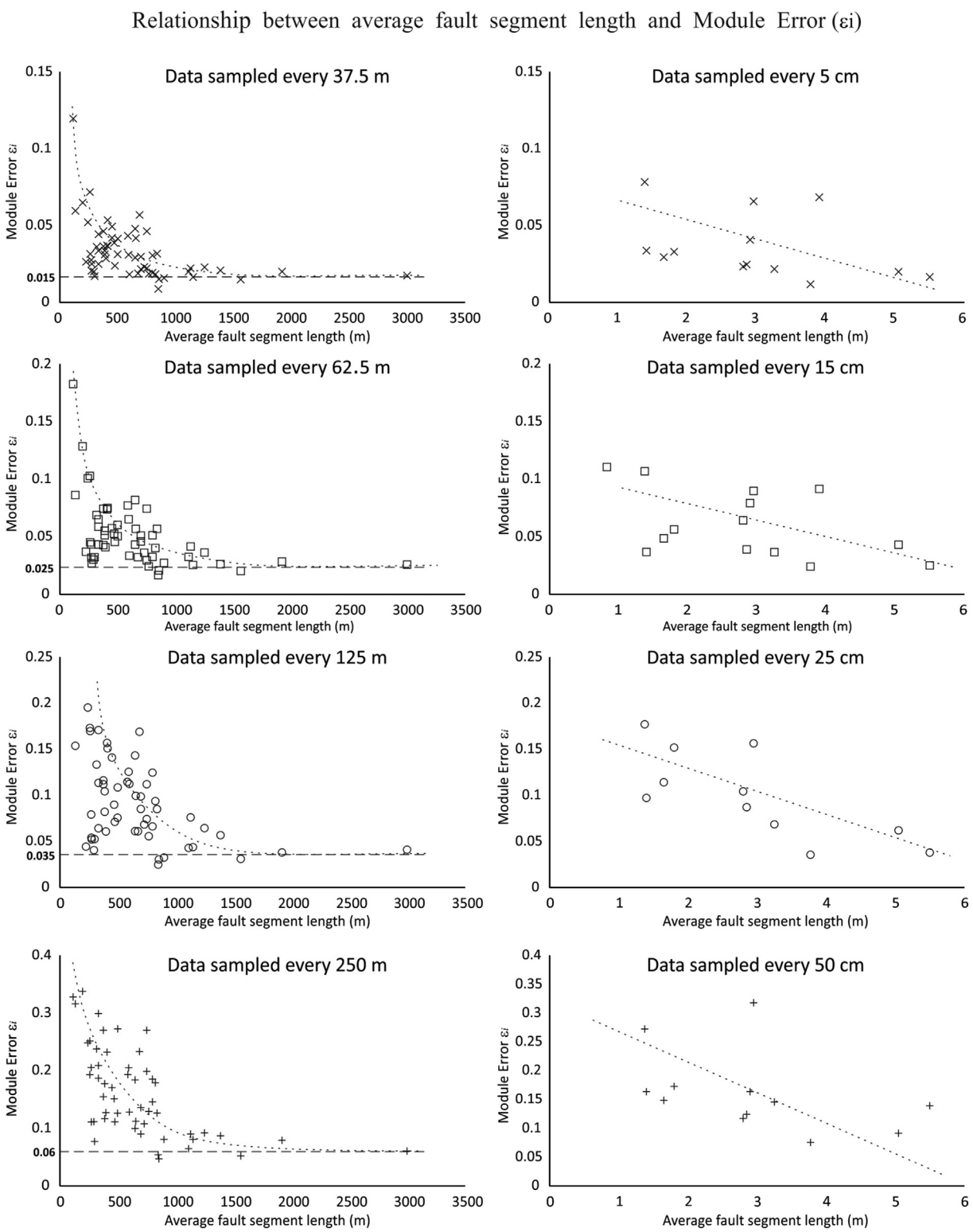

Fig. 12. Relationship between average fault segment length and *Module Error* ε_i for given sampling intervals. All results show that *Module Error* decreases rapidly with longer average fault segment lengths, a character indicating that for smaller fault segment require smaller sampling intervals in order to produce accurate T-D plots.

underestimated. This is especially the case in areas where fault segments are linked, known to form potentially fluid pathways (Reis et al., 2013) (Fig. 14).

Based on our analysis, we suggest the use of fault models reaching maximum data resolution when modelling fault slip tendency and leakage factors. Regardless of the changes increasing sampling intervals have on the interpreted fault roughness and geometry (Yukutake et al., 2014), systematic misinterpretations of fault slip tendency and leakage factor will occur if sampling intervals are not close to maximum data resolution.

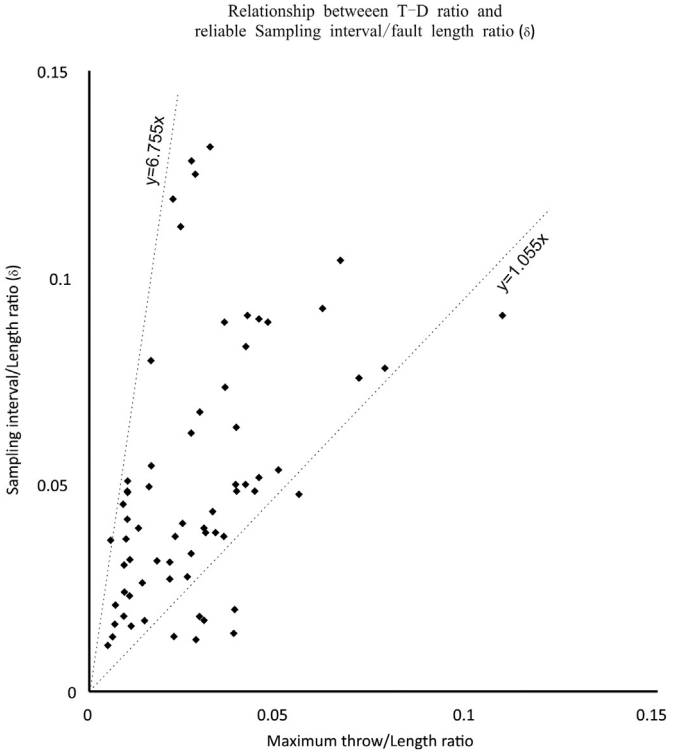

Fig. 13. Relationship between maximum throw/fault length ratio and *Sampling Interval/Fault Length Ratio* (δ). The results roughly suggest a positive relationship insofar as, with a smaller maximum throw/length ratio, a smaller *Sampling Interval/Fault Length Ratio*(δ) should be considered. For a 'constant length' fault growth model, the maximum throw/length ratio increases. Conversely, for an isolated fault, the maximum throw/length ratio decreases or stays constant with subsequent stages of fault growth. Thus, the *Sampling Interval/Fault Length Ratio* (δ) used to produce T-D plots will have significant influence on the subsequent interpretation of fault growth histories.

7.2. Minimum values of δ necessary to constrain the two end-member fault propagation models

When compiling T-D data, *Module Error* (ε_i) increases significantly with increasing sampling intervals (Fig. 9). We thus propose the parameter δ to guide interpreters in the future compilation of T-D plots. In our analysis, the accuracy of compiled T-D plots decreased to 46% when adopting a data sampling interval of 62.5 m on seismic data, i.e. when we collected throw data every 5 inlines/crosslines (Fig. 8). Hence, we strongly suggest that a data sampling of 37.5 m (i.e. every 3 inlines/crosslines, with an accuracy of 92%) is used to compile T-D plots for faults interpreted on 3D seismic data with a maximum horizontal resolution (trace spacing) of 12.5 m. For faults at sub-seismic scales from the Bristol Channel, *accuracy* decreased to 37% when the sampling interval increased to 25 cm, meaning that most T-D plots are inaccurate at relatively small sampling intervals. Hence, a minimum sampling interval of 15 cm is suggested here for the sub-seismic scale faults analysed in the Bristol Channel (Fig. 8). For the rift-related normal faults in Crete, a minimum sampling interval of 100 m is recommended.

Even though our analysis is capable of indicating the ranges of sampling intervals necessary to obtain accurate T-D plots, based on the high-quality seismic data from SE Brazil, researchers and industry use seismic volumes with varied horizontal resolutions. Furthermore, sub-seismic scale faults are also scale variant. We postulate that fixed sampling intervals lose their practical meaning when compiling T-D and T-Z plots for faults that are scale variant, or when their recognition is dependent on the resolution of seismic, remote-sensing or other geophysical data. Fixed sampling intervals also lose their practical meaning when considering individual research aims, e.g. detailed analyses of faults' scale and geometry vs. simple proofs of concept that do not require a systematic collection of throw data. The *Sampling Interval/Fault Length Ratio* δ here proposed addresses the resolution and scale variance in the structural analysis of normal faults. The threshold values of δ suggested below are able to identify first order fault segmentation, which is essential to conduct any reliable fault analyses when using T-D data.

For faults interpreted on seismic data from SE Brazil, with a sampling interval of 12.5 m, a maximum value δ = 0.07 (sampling intervals at < 7% of the fault length) is suggested in this work. For outcropping faults in the Bristol Channel Basin, a δ value of 0.06 (sampling intervals at < 6% of the fault length) is required to obtain accurate T-D plots (Fig. 9). For rift-related faults in SE Crete, a value δ = 0.03 (sampling intervals at < 3% of the fault length) is recommended (Fig. 10c). In Fig. 9, a significant number of measurements are located within the threshold δ values set above, but these measurements are still regarded as innacurate; the reason being that the required δ value necessary to produce reliable T-D plots decreases rapidly with increasing fault length (Fig. 11). We thus suggest a minimum δ of 0.03 (sampling intervals at < 3% of the fault length) for faults that are over 3.5 km long, as the required δ values become relatively constant beyond such a length (Fig. 11). The δ values required to interpret rift-related faults in SE Crete prove that, for the longer faults, interpreters should adopt smaller δ values. However, a minimum value of δ around 0.03 (sampling intervals at < 3% of the fault length) still returns relatively accurate T-D profiles (Fig. 40). For smaller scales of analysis, faults in the Bristol Channel also show a negative relationship with increasing fault length, i.e. smaller δ values should also be applied when fault length increases (Fig. 10b).

This is the first work setting a standard value δ to produce accurate T-D plots at all scales. Our results suggest that for different purposes, the required δ values to produce accurate T-D plots will differ. However, if the aim is to understand fault segmentation and growth patterns, to analyse fault damage zones, or to better characterise the way adjacent faults interact, a *Sampling Interval/Fault Length Ratio* (δ) of 0.05 should be adopted by interpreters and structural geologists by default, without pre-existing knowledge of fault segmentation. This means, in practice, the acquisition of throw (or displacement) data through T-D and T-Z plots at intervals reaching 5% of the total fault length. If this threshold δ value is not adopted, serious underestimations of fault segmentation, fault interaction, fault linkage zone width, and fault damage zones will necessarily occur. The interpreters can then adopt sampling strategies that return more detailed results (e.g. adopting a δ < 0.03) for segmented faults that are longer than 3.5 km, as recommended in the previous paragraphs.

8. Conclusions

Throw-distance (T-D) and throw-depth (T-Z) plots are widely used in fault analyses, particularly when recognising fault segmentation to support the interpretation of fault propagation histories. In parallel, fault slip tendency and leakage factors are often modelled to understand fault sealing properties. Our study presents the first quantitative method that critically assesses the effect of data sampling on the accuracy of T-D and T-Z plots. Outcropping faults of distinct scales, and faults imaged on 3D seismic data, are analysed in this paper to introduce two new parameters; the *Sampling Interval/Fault Length Ratio* (δ) and the *Module Error* (ε_i), used as quantitative parameters to assess the accuracy of fault analyses. Hence, our study reaches the following conclusions:

1) Sampling intervals have a significant influence on the analysis of fault growth histories in multiple ways. With variable sampling intervals: a) fault geometry is significantly changed; b) maximum fault throw values are underestimated; c) fault segments are unrepresented; d) the geometry of fault linkage zones is changed; e)

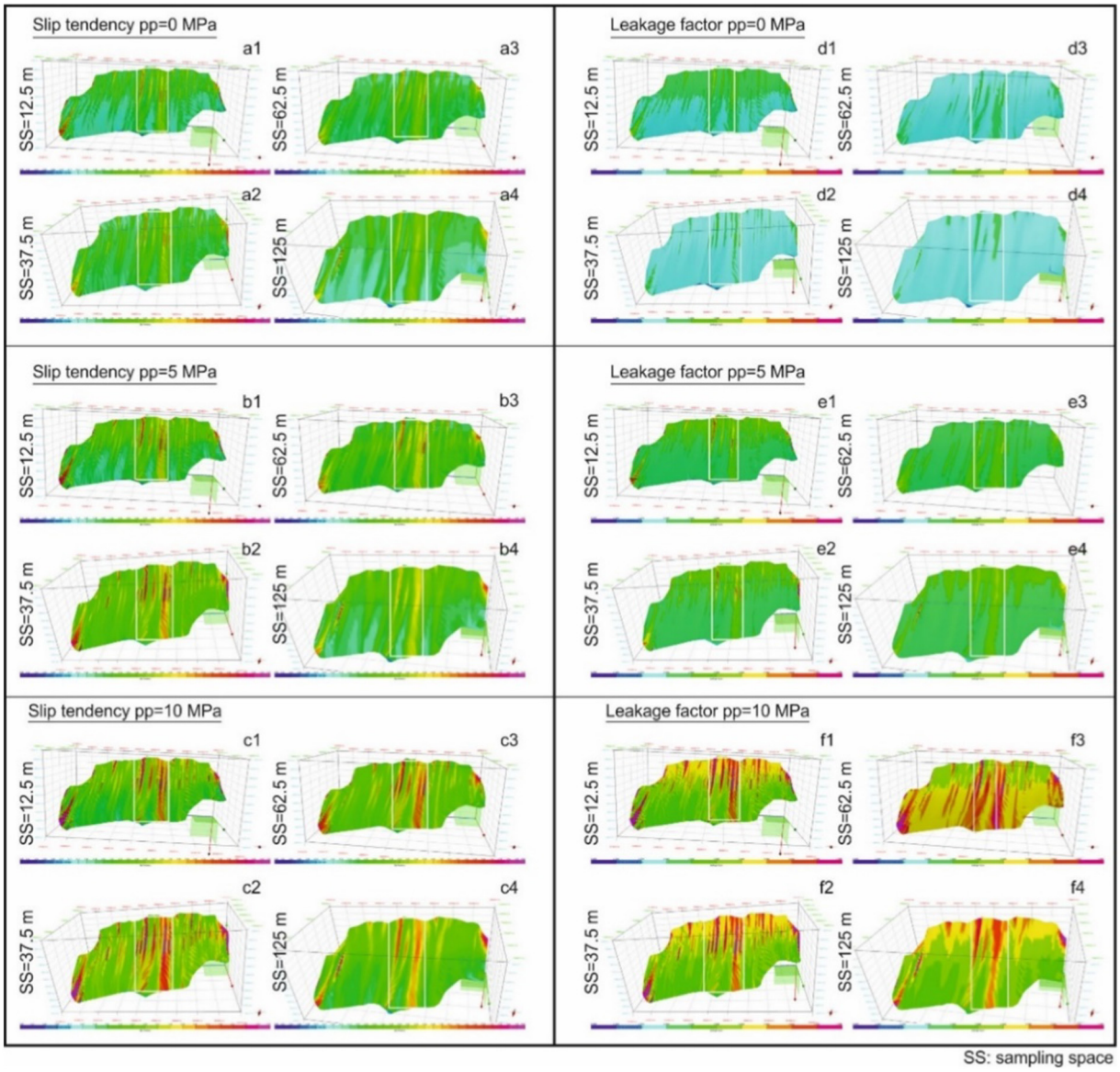

Fig. 14. Influence of variable sampling intervals on fault slip tendency and leakage factor analyses. Left) slip tendency analysis under pore-pressures of 0 MPa, 5 MPa and 10 MPa with different sampling intervals. Right) leakage factor analysis under pore pressures of 0 MPa, 5 MPa and 10 MPa with different sampling intervals. White boxes in the figures refer to the segment linkage zone, where higher slip tendency and leakage factors occur. a1–a4) Slip tendency under pore-pressure of 0 MPa. With increasing sampling intervals, the magnitude of slip tendency decreases (a2–a4). In figures a2 and a3, slip tendency at the lower part of the fault is underestimated. In Figure a4, fault surface becomes smooth with a sampling interval of 125 m, that areas of higher slip tendency are blurred. In b1–b4, c1–c4) slip tendency under a pore-pressure of 5 MPa is similar to that of hydrostatic pore pressure; both the magnitude and the distribution of slip tendency are significantly changed with larger sampling intervals. d1–d4) Leakage factor analysis under hydrostatic conditions, with leakage factors in the upper half of the fault being systematically underestimated, and zones with the highest leakage factors being also underestimated with coarser sampling intervals. e1–e4) Leakage factor under a pore-pressure of 5 MPa shows similar results to that under hydrostatic conditions. f1–f4) With a pore pressure of 10 MPa, a sampling interval of 37.5 m (f2) shows similar results to a sampling interval of 12.5 m (f1), except that the magnitude of leakage factor is relatively smaller. When the sampling interval increases to 62.5 m, the lower part of the fault shows abnormally high leakage factor values (f3). Areas with high leakage factors are blurred and markedly different from those obtained with a sampling interval of 12.5 m (f1). When the sampling interval increases to 125 m, leakage factors are systematically underestimated (f4).

the width of fault linkage zone is underestimated; f) fault interaction zones are lost. This means, in effect, that methods based on Expansion Indexes (EI) and isochron mapping are unreliable beyond certain scales of analysis, i.e. beyond line-by-line (maximum seismic resolution) interpretation (see also Alves, 2012).

2) Using the SE Brazil seismic data, the accuracy in T-D plots is quantitatively lost when sampling intervals are larger than 37.5 m (every 3 shot-points for a common 3D seismic volume, with a bin spacing of 12.5 m). This sampling interval adopted by interpreters, however, should differ depending on the horizontal resolution (or bin size) of the seismic data used and the total length of faults.

3) *Module Error* (ε_i) decreases rapidly with longer average fault-segment lengths. This ε_i value should be well under 0.06 to avoid any of the major caveats associated with poor data sampling.

4) A δ value of 0.05 is therefore recommended for structural analyses undertaken without prior knowledge of fault segmentation, and for fault lengths < 3500 m. This signifies the sampling of throws at intervals < 5% of the total length of faults.

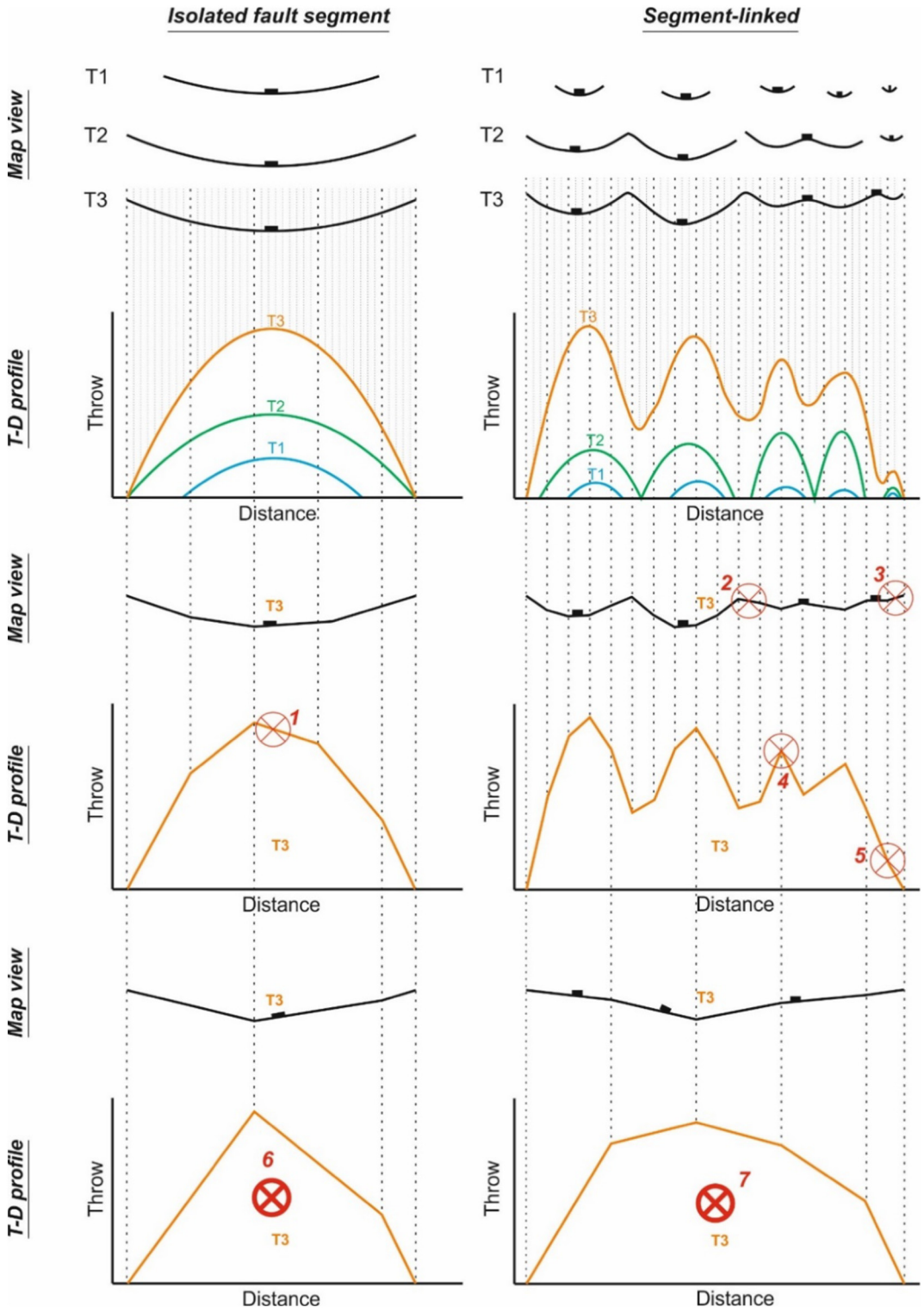

Fig. 15. Schematic representation of the impact of data sampling on fault analyses. At coarser sampling intervals: 1. fault geometry is changed from symmetric to asymmetric. 2. The geometry of fault linkage zone is significantly changed. 3. The geometry of an entire fault segment is changed. 4. Fault-linkage zone geometry and width are significantly changed. 5. Fault segments are not discerned.

5) A threshold δ value of 0.03 is suggested for faults longer than 3500 m. This signifies, in practice, the acquisition of throw data at distances that are < 3% of the total length of the fault.

6) For detailed fault slip tendency and leakage factor analyses, a δ value reaching maximum data resolution is strongly suggested so that interpreters avoid systematic misinterpretations of fault slip and leakage properties. This means undertaking T-Z measurements and interpreting fault sticks at every single seismic trace. It also favours the use of LIDAR data (or very small sampling distances) in field-based analyses.

Acknowledgments

We thank CGG for the permission to use the seismic data in this paper. Schlumberger (Petrel®), Midland Valley (Move®) and the Southwest Research Institute (3D Stress®) are acknowledged for the provision of using the related software in completing this piece of work. We acknowledge the contributions of I. Watkinson, an anonymous reviewer, and Tectonophysics editor Kelin Wang, which greatly improved the quality of this work. Tao Ze also thanks the China Scholarship Council (CSC) for supporting the Ph.D. project from which this work has been derived. The authors thank the colleagues in the 3D Seismic Lab at Cardiff University for the help and tips provided.

Appendix A. Supplementary data

Supplementary data to this article can be found online at https://doi.org/10.1016/j.tecto.2019.03.013.

References

Alves, T.M., 2012. Scale-relationships and geometry of normal faults reactivated during gravitational gliding of Albian rafts (Espírito Santo Basin, SE Brazil). Earth Planet. Sci. Lett. 331-332, 80–96.
Alves, T.M., Cupkovic, T., 2018. Footwall degradation styles and associated sedimentary facies distribution in SE Crete: Insights into tilt-block extensional basins on continental margins. Sediment. Geol. 367, 1–19.
Athmer, W., Luthi, S.M., 2011. The effect of relay ramps on sediment routes and deposition: a review. Sediment. Geol. 242, 1–17.
Bahorich, M., Farmer, S., 1995. 3-D seismic discontinuity for faults and stratigraphic features: the coherence cube. Lead. Edge 14, 1053–1058.
Barnett, J.A.M., Mortimer, J., Rippon, J.H., Walsh, J.J., Watterson, J., 1987. Displacement geometry in the volume containing a single normal fault. Am. Assoc. Pet. Geol. Bull. 71, 925–937.
Baudon, C., Cartwright, J., 2008a. 3D seismic characterisation of an array of blind normal faults in the Levant Basin, Eastern Mediterranean. J. Struct. Geol. 30, 746–760.
Baudon, C., Cartwright, J., 2008b. Early stage evolution of growth faults: 3D seismic insights from the Levant Basin, Eastern Mediterranean. J. Struct. Geol. 30, 888–898.
Baudon, C., Cartwright, J., 2008c. The kinematics of reactivation of normal faults using high resolution throw mapping. J. Struct. Geol. 30, 1072–1084.
Booth-Rea, G., Azañón, J.-M., Azor, A., García-Dueñas, V.C., 2004. Influence of strike-slip fault segmentation on drainage evolution and topography. A case study: the Palomares Fault Zone (southeastern Betics, Spain). J. Struct. Geol. 26, 1615–1632.
Caputo, R., Catalano, S., Monaco, C., Romagnoli, G., Tortorici, G., Tortorici, L., 2010. Active faulting on the island of Crete (Greece). Geophys. J. Int. 183, 111–126.
Cartwright, J.A., Trudgill, B.D., Mansfield, C.S., 1995. Fault growth by segment linkage: an explanation for scatter in maximum displacement and trace length data from the Canyonlands Grabens of SE Utah. J. Struct. Geol. 17, 1319–1326.
Cartwright, J., Trudgill, B., Mansfield, C., 2000. Fault growth by segment linkage: an explanation for scatter in maximum displacement and trace length data from the Canyonlands grabens of SE Utah: Reply. J. Struct. Geol. 22, 141–143.
Childs, C., Watterson, J., Walsh, J., 1995. Fault overlap zones within developing normal fault systems. J. Geol. Soc. 152, 535–549.
Childs, C., Nicol, A., Walsh, J., Watterson, J., 2003. The growth and propagation of synsedimentary faults. J. Struct. Geol. 25, 633–648.
Choi, J.H., Yang, S.J., Han, S.R., Kim, Y.S., 2015. Fault zone evolution during Cenozoic tectonic inversion in SE Korea. J. Asian Earth Sci. 98, 167–177.
Cowie, P.A., Scholz, C.H., 1992. Physical explanation for the displacement-length relationship of faults using a post-yield fracture mechanics model. J. Struct. Geol. 14, 1133–1148.
Dart, C.J., McClay, K., Hollings, P.N., 1995. 3D analysis of inverted extensional fault systems, southern Bristol Channel basin, UK. Geol. Soc. Lond., Spec. Publ. 88, 393.
Finch, E., Gawthorpe, R.L., 2017. Growth and interaction of normal faults and fault network evolution in rifts: insights from three-dimensional discrete element modelling. In: Childs, C., Holdsworth, R.E., Jackson, C.A.-L., Manzocchi, T., Walsh, J.J., Yielding, G. (Eds.), Geological Society, London, Special Publications. 439https://doi.org/10.1144/SP439.23.
Fossen, H., Rotevatn, A., 2016. Fault linkage and relay structures in extensional settings—a review. Earth Sci. Rev. 154, 14–28.
Gaki-Papanastassiou, K., Karymbalis, E., Papanastassiou, D., Maroukian, H., 2009. Quaternary marine terraces as indicators of neotectonic activity of the Ierapetra normal fault SE Crete (Greece). Geomorphology 104, 38–46.
Giba, M., Walsh, J.J., Nicol, A., 2012. Segmentation and growth of an obliquely reactivated normal fault. J. Struct. Geol. 39, 253–267.
Glen, R.A., Hancock, P.L., Whittaker, A., 2005. Basin inversion by distributed deformation: the southern margin of the Bristol Channel Basin, England. J. Struct. Geol. 27, 2113–2134.
Gupta, S., Cowie, P., Dawers, N.H., Underhill, J.R., 1998. A mechanism to explain rift-basin subsidence and stratigraphic patterns through fault-array evolution. Geology 26 (7), 595–598.
Hemelsdaël, R., Ford, M., 2016. Relay zone evolution: a history of repeated fault propagation and linkage, central Corinth rift, Greece. Basin Res. 28, 34–56.
Imber, J., Childs, C., Nell, P.A.R., Walsh, J.J., Imber, D., Childs, S., Walsh, S., Nell, S., Hodgetts, S., Flint, S., 2002. Hanging wall fault kinematics and footwall collapse in listric growth fault systems. J. Struct. Geol. 25, 197–208.
Jackson, C.A.L., Rotevatn, A., 2013. 3D seismic analysis of the structure and evolution of a salt-influenced normal fault zone: a test of competing fault growth models. J. Struct. Geol. 54, 215–234.
Jackson, C.A.-L., Bell, R.E., Rotevatn, A., Tvedt, A.B., 2017. Techniques to determine the kinematics of synsedimentary normal faults and implications for fault growth models. Geol. Soc. Lond., Spec. Publ. 439, SP439. 422.
Jung, N., Han, W., Watson, Z., Graham, J.P., Kim, K., 2014. Fault-controlled CO_2 leakage from natural reservoirs in the Colorado Plateau, East-Central Utah. Earth Planet. Sci. Lett. 403, 358–367.
Kim, Y.-S., Sanderson, D.J., 2005. The relationship between displacement and length of faults: a review. Earth-Sci. Rev. 68, 317–334.
Lohr, T., Krawczyk, C.M., Oncken, O., Tanner, D.C., 2008. Evolution of a fault surface from 3D attribute analysis and displacement measurements. J. Struct. Geol. 30, 690–700.
Long, W., Li, Z.Q., Li, Y., et al., 2018. Experimental Insights on the Structural Patterns and Their Formation Mechanisms of the Xujiaweizi Fault Depression in the Songliao Basin. J. Earth Sci. 29 (2), 369–375.
Mansfield, C., Cartwright, J., 2001. Fault growth by linkage: Observations and implications from analogue models. J. Struct. Geol. 23, 745–763.
Manzocchi, T., Childs, C., Walsh, J.J., 2010. Faults and fault properties in hydrocarbon flow models. Geofluids 10, 94–113.
Mason, J., Schneiderwind, S., Pallikarakis, A., Wiatr, T., Mechernich, S., Papanikolaou, I., Reicherter, K., 2016. Fault structure and deformation rates at the Lastros-Sfaka Graben, Crete. Tectonophysics 683, 216–232.
Mattos, N.H., Alves, T.M., Omosanya, K.O., 2016. Crestal fault geometries reveal late halokinesis and collapse of the Samson Dome, Northern Norway: Implications for petroleum systems in the Barents Sea. Tectonophysics 690, 76–96.
Mohammedyasin, S., Lippard, S., Omosanya, K., Johansen, S., Harishidayat, D., 2016. Deep-seated faults and hydrocarbon leakage in the Snøhvit Gas Field, Hammerfest Basin, Southwestern Barents Sea. Mar. Pet. Geol. 77, 160–178.
Morley, C.K., 1999. Patterns of displacement along large normal faults: Implications for basin evolution and fault propagation, based on examples from East Africa. Bull. Am. Assoc. Pet. Geol. 83, 613–634.
Morley, C., Nelson, R., Patton, T., Munn, S., 1990. Transfer zones in the East African rift system and their relevance to hydrocarbon exploration in rifts (1). AAPG Bull. 74, 1234–1253.
Morris, A., Ferrill, D.A., Henderson, D.B., 1996. Slip-tendency analysis and fault reactivation. Geology 24, 275–278.
Muraoka, H., Kamata, H., 1983. Displacement distribution along minor fault traces. J. Struct. Geol. 5, 483–495.
Peacock, D.C.P., Sanderson, D.J., 1991. Displacements, segment linkage and relay ramps in normal fault zones. J. Struct. Geol. 13, 721–733.
Peacock, D.C.P., Nixon, C.W., Rotevatn, A., Sanderson, D.J., Zuluaga, L.F., 2017. Interacting faults. J. Struct. Geol. 97, 1–22.
Pei, Y., Paton, D.A., Knipe, R.J., Wu, K., 2015. A review of fault sealing behaviour and its evaluation in siliciclastic rocks. Earth Sci. Rev. 150, 121–138.
Pizzi, A., Galadini, F., 2009. Pre-existing cross-structures and active fault segmentation in the northern-central Apennines (Italy). Tectonophysics 476, 304–319.
Polit, A.T., Schultz, R.A., Soliva, R., 2009. Geometry, displacement–length scaling, and extensional strain of normal faults on Mars with inferences on mechanical stratigraphy of the Martian crust. J. Struct. Geol. 31, 662–673.
Rawnsley, K. D., Peacock, D. C. P., Rives, T., Petit, J. P., 1998. Joints in the Mesozoic sediments around the Bristol Channel Basin. J. Struct. Geol. 2012, 1641–1661.
Reis, Á.F.C., Bezerra, F.H.R., Ferreira, J.M., do Nascimento, A.F., Lima, C.C., 2013. Stress magnitude and orientation in the Potiguar Basin, Brazil: Implications on faulting style and reactivation. Journal of Geophysical Research: Solid Earth 118, 5550–5563.
Rotevatn, A., Jackson, C.A.L., Tvedt, A.B.M., Bell, R.E., Blækkan, l., 2018. How do normal faults grow? J. Struct. Geol (In press).
Ryan, L., Magee, C., Jackson, C.A.-L., 2017. The kinematics of normal faults in the Ceduna Subbasin, offshore southern Australia: Implications for hydrocarbon trapping in a frontier basin. AAPG Bull. 101, 321–341.
Schlische, R.W., Withjack, M.O., 2009. Origin of fault domains and fault-domain boundaries (transfer zones and accommodation zones) in extensional provinces: result of random nucleation and self-organized fault growth. J. Struct. Geol. 31, 910–925.
Seebeck, H., Nicol, A., Beetham, J.J., Seebeck, C., Pettinga, R.D., Walsh, J., Childs, J., 2014. Fluid flow in fault zones from an active rift. J. Struct. Geol. 62, 52–64.
Taylor, S.K., Nicol, A., Walsh, J.J., 2008. Sediment compaction of normal displacements on growth faults. J. Struct. Geol. 30, 394–405.
Torabi, A., Berg, S.S., 2011. Scaling of fault attributes: a review. Mar. Pet. Geol. 28, 1444–1460.
Torabi, A., Alaei, B., Libak, A., 2019. Normal fault 3D geometry and displacement revisited: Insights from faults in the Norwegian Barents Sea. Mar. Pet. Geol. 99, 135–155.
Turko, J.M., Knuepfer, P.L., 1991. Late Quaternary fault segmentation from analysis of scarp morphology. Geology 19, 718–721.
Tvedt, A.B.M., Rotevatn, A., Jackson, C.A.L., 2016. Supra-salt normal fault growth during the rise and fall of a diapir: perspectives from 3D seismic reflection data, Norwegian North Sea. J. Struct. Geol. 91, 1–26.
Underhill, J.R., Paterson, S., 1998. Genesis of tectonic inversion structures: seismic evidence for the development of key structures along the Purbeck–Isle of Wight Disturbance. J. Geol. Soc. 155, 975.

Valley, M., 2014. Midland Valley Move Application.
Van Gent, H., Back, S., Urai, J.L., Kukla, P., 2010. Small-scale faulting in the Upper Cretaceous of the Groningen block (the Netherlands): 3D seismic interpretation, fault plane analysis and regional paleostress. J. Struct. Geol. 32, 537–553.
Walsh, J., Nicol, A., Childs, C., 2002. An alternative model for the growth of faults. J. Struct. Geol. 24, 1669–1675.
Walsh, J., Bailey, W., Childs, C., Nicol, A., Bonson, C., 2003. Formation of segmented normal faults: a 3-D perspective. J. Struct. Geol. 25, 1251–1262.
Ward, N.I.P., Alves, T.M., Blenkinsop, T.G., 2016. Reservoir leakage along concentric faults in the Southern North Sea: implications for the deployment of CCS and EOR techniques. Tectonophysics 690, 97–116.
Watterson, J., Walsh, J.J., Gillespie, P.A., Easton, S., 1996. Scaling systematics of fault sizes on a large scale range fault map. J. Struct. Geol. 18, 199–214.
Whittaker, A.C., Walker, A.S., 2015. Geomorphic constraints on fault throw rates and linkage times: examples from the Northern Gulf of Evia, Greece. Journal of Geophysical Research-Earth Surface 120, 137–158.
Wilson, P., Elliott, G.M., Gawthorpe, R.L., Jackson, C.A.L., Michelsen, L., Sharp, I.R., 2013. Geometry and segmentation of an evaporite-detached normal fault array: 3D seismic analysis of the southern Bremstein Fault Complex, offshore mid-Norway. J. Struct. Geol. 51, 74–91.
Worum, G., van Wees, J.D., Bada, G., van Balen, R.T., Cloetingh, S., Pagnier, H., 2004. Slip tendency analysis as a tool to constrain fault reactivation - a numerical approach applied to three-dimensional fault models in the Roer Valley rift system (southeast Netherlands). Journal of Geophysical Research: Solid Earth (1978–2012) 109.
Yukutake, Y., Takeda, T., Yoshida, A., 2014. The applicability of frictional reactivation theory to active faults in Japan based on slip tendency analysis. Earth Planet. Sci. Lett. 411, 188–198.
Ze, T., Alves, T.M., 2016. The role of gravitational collapse in controlling the evolution of crestal fault systems (Espírito Santo Basin, SE Brazil). J. Struct. Geol. 92, 79–98.
Ze, T., Alves, T.M., 2017. The role of gravitational collapse in controlling the evolution of crestal fault systems (Espírito Santo Basin, SE Brazil)–Reply. J. Struct. Geol. 98, 12–14.
Zhang, P., Slemmons, D., Mao, F., 1991. Geometric pattern, rupture termination and fault segmentation of the Dixie Valley—Pleasant Valley active normal fault system, Nevada, USA. J. Struct. Geol. 13, 165–176.